European Journal of Medicinal Chemistry 132 (2017) 90–107

Contents lists available at ScienceDirect

European Journal of Medicinal Chemistry

journal homepage: http://www.elsevier.com/locate/ejmech

Research paper

Using gene expression database to uncover biology functions of 1,4-disubstituted 1,2,3-triazole analogues synthesized via a copper (I)-catalyzed reaction

Chun-Li Su [a, *, 1], Chia-Ling Tseng [a, 1], Chintakunta Ramesh [b, 1], Hsiao-Sheng Liu [c, d], Chi-Ying F. Huang [e, f, **], Ching-Fa Yao [b, ***]

[a] Department of Human Development and Family Studies, National Taiwan Normal University, Taipei 106, Taiwan
[b] Department of Chemistry, National Taiwan Normal University, Taipei 116, Taiwan
[c] Department of Microbiology and Immunology, College of Medicine, National Cheng Kung University, Tainan 701, Taiwan
[d] Center of Infectious Disease and Signaling Research Center, College of Medicine, National Cheng Kung University, Tainan 701, Taiwan
[e] Institute of Biopharmaceutical Sciences, National Yang-Ming University, Taipei 112, Taiwan
[f] Department of Biochemistry, College of Medicine, Kaohsiung Medical University, Kaohsiung 807, Taiwan

ARTICLE INFO

Article history:
Received 12 January 2017
Received in revised form
14 March 2017
Accepted 15 March 2017
Available online 18 March 2017

Keywords:
1,4-Disubstituted 1,2,3-triazole analogues
L1000 gene expression profiling
Connectivity map
Apoptosis
Autophagy
Sorafenib

ABSTRACT

We have synthesized bioactive 1,4-disubstituted 1,2,3-triazole analogues containing 2*H*-1,4-benzoxazin-3-(4*H*)-one derivatives via 1,3-dipolar cycloaddition in the presence of CuI. All the reactions proceeded smoothly and afforded its desired products in excellent yields. Among these analogues, **3y** exhibited a better cytotoxic effect on human hepatocellular carcinoma (HCC) Hep 3B cells and displayed less cytotoxicity on normal human umbilical vein endothelial cells, compared with Sorafenib, a targeted therapy for advanced HCC. **3y** also induced stronger apoptosis and autophagy. Addition of curcumin enhanced **3y**-induced cytotoxicity by further induction of autophagy. Using gene expression signatures of **3y** to query Connectivity Map, a glycogen synthase kinase-3 inhibitor (AR-A014418) was predicted to display similar molecular action of **3y**. Experiments further demonstrate that AR-A014418 acted like **3y**, and *vice versa*. Overall, our data suggest the chemotherapeutic potential of **3y** on HCC.

1. Introduction

1,2,3-triazoles exhibit a wide spectrum of biological properties such as anti-bacterial, anti-allergic, anti-fungal, anti-epileptic and anti-HIV activity [1–6]. Additionally, 1,2,3-triazoles have widespread applications as light stabilizers, corrosion retarding agents, fluorescent whiteners, and optical brighteners [7]. Consequently, synthetic approaches toward 1,2,3-triazoles have attracted significant attention [8–13]. Over the past few years, copper (I)-catalyzed azide-alkyne cycloaddition (CuAAC) has received considerable attention with respect to its use in the construction of 1,4-disubstituted 1*H*-1,2,3-triazoles due to a number of advantages it possesses which include high regioselectivity, high quantitative product yields, a broad range of substrate scope, and mild reaction conditions [14,15]. Meldal and Sharpless independently reported the 1,3-dipolar cycloaddition of alkyne and azide in the presence of a catalytic amount of Cu(I)-catalyst in early 2002 [14–17]. After this discovery, the cycloaddition reaction has been well utilized for the synthesis of various novel 1,2,3-triazoles including fused triazoles [2,18–29], triazolo heterocyclic frameworks [6,19,30–36], and macrocyclic triazoles [37–42]. This click chemistry is a widely utilized application in peptide chemistry [43–50], as well as in carbohydrate chemistry [51–59].

Abbreviations: AO, acridine orange; AVOs, acidic vesicular organelles; C-Map, connectivity Map; CuAAC, copper (I)-catalyzed azide-alkyne cycloaddition; DMEM, Dulbecco's modified Eagle medium; DMSO, dimethyl sulfoxide; FDA, the U.S. Food and Drug Administration; GSK-3, glycogen synthase kinase-3; HCC, hepatocellular carcinoma; HUVEC, human umbilical vein endothelial cells; IC_{50}, the 50% inhibitory concentration; MTT, 3-[4,5-Dimethylthiazol-2-yl]-2,5-diphenyltetrazolium bromide; PI, propidium iodide; SEMs, standard errors of the means.

* Corresponding author.
** Corresponding author.
*** Corresponding author.
E-mail addresses: chunlisu@ntnu.edu.tw (C.-L. Su), cyhuang5@ym.edu.tw (C.-Y.F. Huang), cheyaocf@ntnu.edu.tw (C.-F. Yao).
[1] These authors contributed equally to this work.

http://dx.doi.org/10.1016/j.ejmech.2017.03.034
0223-5234/

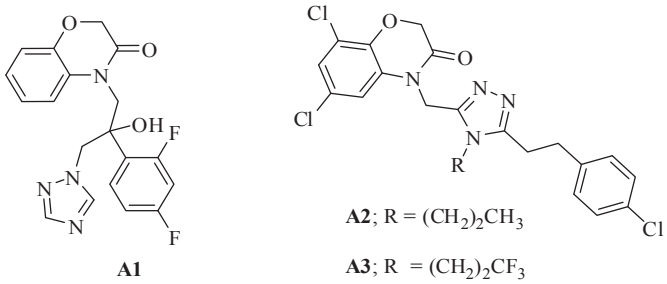

Scheme 1. Some of the biologically important structures of the 2*H*-1,4-benzox azin-3-(4*H*)-one analogues containing triazole moieties.

Furthermore, 2*H*-1,4-benzoxazin-3-(4*H*)-one and its derivatives are ubiquitous heterocyclic compounds known to possess a range of biological and medicinal properties including anti-pyretic, anti-inflammatory, anti-hypertensive, and anti-ulcer effects, and have been used as potassium channel modulators, anti-rheumatic agents, and plant resistance factors against microbial diseases and insects [60–66]. Of particular interest are the 2*H*-1,4-benzoxazin-3-(4*H*)-one analogues containing azoles and their derivatives, which display anti-fungal activity against *Candida albicans* [60,63,67–70]. Examples of the 2*H*-1,4-benzoxazin-3-(4*H*)-one analogues containing triazole and their derivatives are presented in Scheme 1. Among these selected examples, compound **A1** is a novel class of *anti-Candida* agent, which exhibits excellent anti-*Candida*

Table 1
Investigation of solvent effect on the model reaction between alkyne and azide.

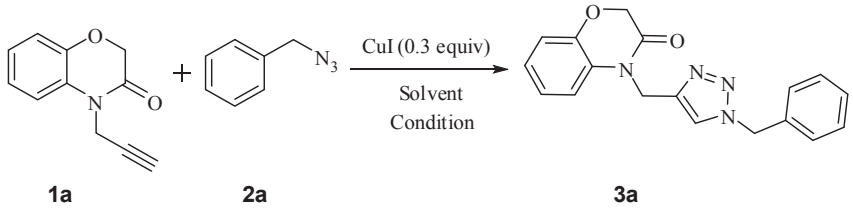

Entry	Solvent	Condition	Time	Yield of **3a** (%)[a,c]
1	1,4-dioxane	rt	13 h	93
2	DMSO	rt	1 h	73
3	DMF	rt	3 h	69
4	DMSO	100 °C	24 h	—[b]
5	ACN	reflux	5 h	71
6	THF	reflux	6 h	68
7	Toluene	80 °C	8 h	63
8	EtOH	reflux	24 h	65
9	H_2O	80 °C	40 min	73
10	Neat	80 °C	1 h	53
11	**1,4-dioxane**	**80°C**	**45 min**	**97**

[a] All the reactions were carried out on 1.0 mmole scale.
[b] Reaction was carried out in the absence of CuI.
[c] Isolated yields.

Table 2
Examination of various copper catalysts and amount of catalyst on the model reaction between alkyne and azide.

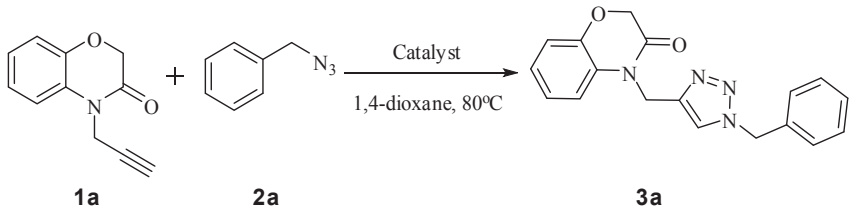

Entry	Catalyst	Equivalent	Time	Yield of **3a** (%)[a,c]
1	none	–	24 h	——[b]
2	$CuSO_4 \cdot 5H_2O$	0.3	24 h	trace[b]
3	$Cu(OAc)_2$	0.3	1 h	89
4	$Cu(acac)_2$	0.3	1 h	87
5	CuCl	0.3	1 h	82
6	CuBr	0.3	1 h	86
7	CuI	0.05	3.5 h	91
8	CuI	0.1	3 h	92
9	CuI	0.15	2.5 h	92
10	CuI	0.2	1.5 h	94
11	**CuI**	**0.3**	**45 min**	**97**

[a] All the reactions carried out on 1.0 mmole scale.
[b] Recovered starting materials.
[c] Isolated yields.

activity, as recently reported by Borate et al. [67]. Similarly, compounds **A2** and **A3** are non-glucoside potent and are highly selective sodium glucose co-transporter 2 (SGLT2) inhibitors (a diabetes drug) [68]. Several diabetes drugs have been shown anti-cancer activity with high dose in many cancer cell lines. Hence, 2*H*-1,4-benzoxazin-3-(4*H*)-one and triazole moieties provide us new pharmacophors for compound modification against cancer cells.

Human HCC is the fifth most common cancer and the third leading cause of cancer-related death in the world [71]. More than 75% of the cases occur in the Asia-Pacific region. Patients with HCC have a poor prognosis and die within several months of diagnosis [72]. Chemotherapy and surgery are the primary ways to deal with

Table 3
Scope of the reaction with respect to alkyne.[a,b,c]

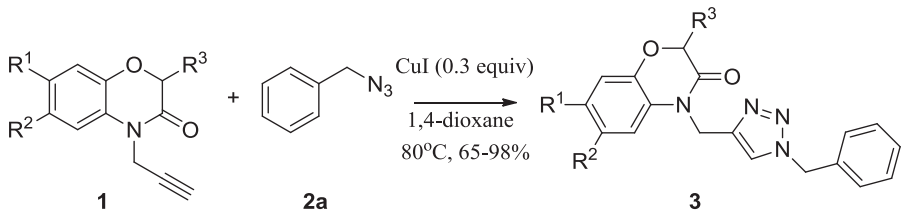

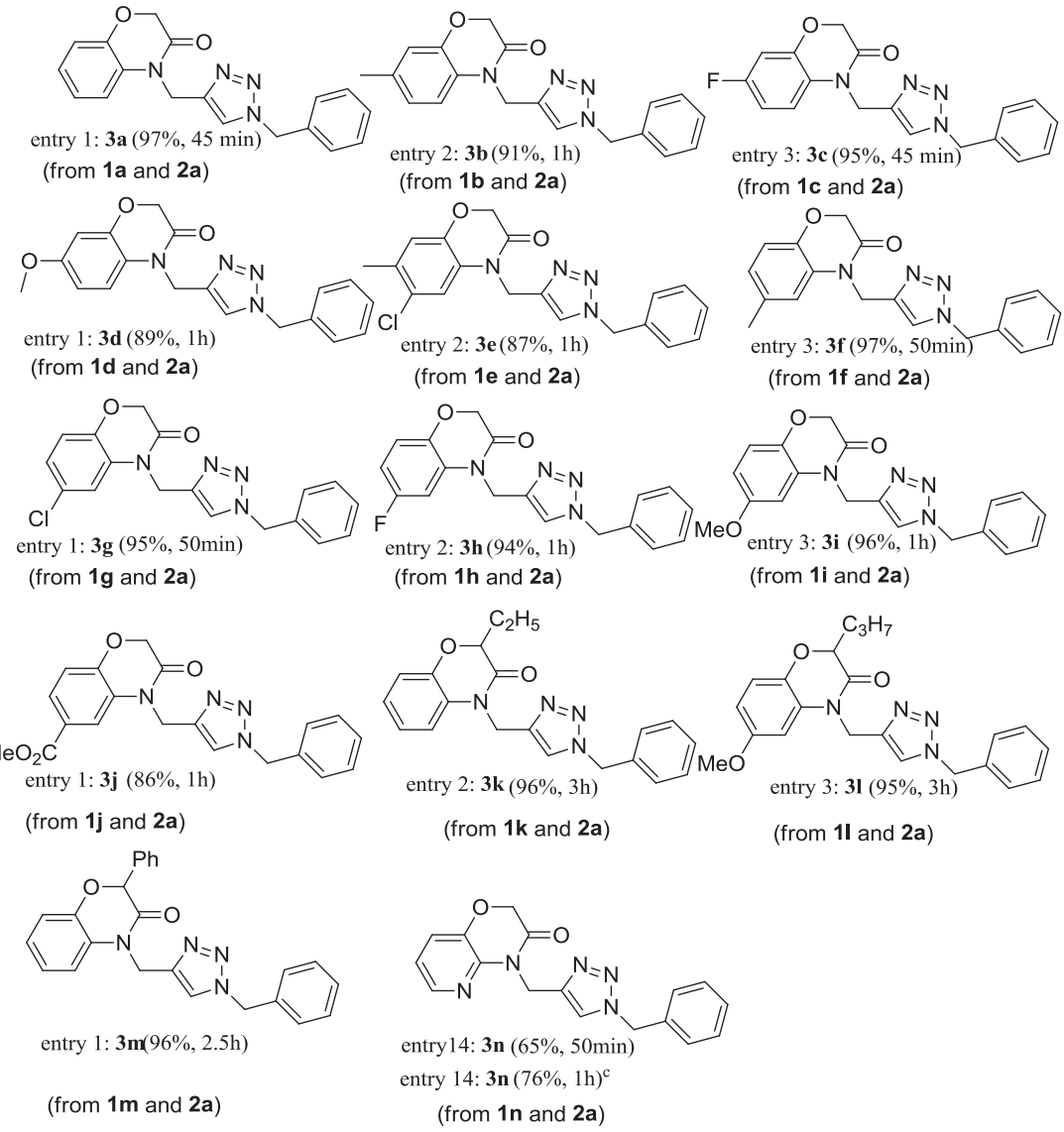

[a] All the reactions were carried out on 1mmole scale.
[b] Isolated yields.
[c] Reaction in the presence of DIPEA.

HCC. However, anti-cancer therapy for HCC is still limited by intrinsic drug resistance [73]. Sorafenib, an oral multikinase inhibitor with anti-proliferation and anti-angiogenic properties [74], is an U.S. Food and Drug Administration (FDA)-approved drug for advanced renal cancer and is also the only FDA-approved targeted therapy for advanced HCC [75]. Sorafenib has also been demonstrated to inhibit the proliferation of many other human cancer cells such as non-small cell lung cancer, breast, colon, and pancreas cancers [76,77]. Inhibition of serine/threonine kinase c-Raf and b-Raf, platelet-derived growth factor receptor-α and β, cytokine receptor c-KIT, and the receptor tyrosine kinases Flt-3 by Sorafenib has been observed [78–80]. Nevertheless, Sorafenib only improved overall survival by nearly 3 months in patients with advanced HCC [81], and the improvement seems to be poor for those with hepatitis B [82]. Moreover, it seems to have a distinct adverse effect profile and reduces patients' quality of life. A meta-analysis of clinical trials shows that patients who took Sorafenib had many undesirable side effects, including increases in the risk of hypertension, bleeding, and arterial thromboembolism [83–86]. Major side effects, such as diarrhea, fatigue, and hand-foot syndrome, increased in patients with advanced cirrhosis and in those who received combination therapy of Sorafenib and 5-fluorouracil [82]. Therefore, there is an urgent need to develop novel therapeutic agents for treatment of HCC.

Due to the shortage of new drugs for treating cancers and the rising expense of drug development, methodologies that allow the exploration of associations among diseases, genes, and chemical expression profiles may yield potential therapeutic targets. The Connectivity Map (C-Map) is a database containing the gene expression profiles of 4 different cancer cells treated with 1309 drugs, including FDA-approved drugs and other small molecules [87,88]. Thus, C-Map provides information indicating which genes were up- or down-regulated by FDA-approved drugs and/or other small molecules. We hypothesized that if a compound displays a similar gene expression profile to that of an FDA-approved drug on the C-Map, the compound may have similar molecular mechanisms to those of the FDA-approved drug. In our recent publications, we demonstrated that, using gene expression signatures to query C-Map, a small molecule (Trifluoperazine, an anti-psychotic agent; Antimycin A, an anti-fungal agent) exhibited an anti-tumor effect and enabled lung cancer stem-like cells to overcome drug resistance *in vitro* and *in vivo* [89,90]. The target identification of new compounds based on 2*H*-1,4-benzoxazin-3-(4*H*)-one and triazoles moiety is an ideal example by applying C-Map.

Programmed cell death can be divided into two main categories: apoptosis (Type I) and autophagy (Type II). Insufficient apoptosis contributes to the pathogenesis of cancer, and induction of apoptosis has been suggested to be a promising strategy for treating cancers [91]. Typical morphological features of apoptotic cell death are condensed chromatin in the nucleus, DNA fragmentation, phosphatidylserine externalization, and generation of apoptotic bodies [92]. Autophagy is also a normal physiological process. The dynamic process of autophagy involves protein degradation and recycling of injured organelles during nutrient starvation and stress [93]. Recent studies on autophagy-induced death of breast, colon, prostate, and brain cancer cells in various anti-cancer therapies, such as chemotherapy, irradiation, and hyperthermia, have renewed interest in autophagy in the field of oncology [94,95].

In the present study, the newly synthesized novel compounds were examined for their anti-cancer potential. Induction of apoptosis and autophagy was examined. Our results indicate that **3y** at a lower concentration exhibited a better cytotoxic effect than that of Sorafenib on human HCC cells via induction of apoptosis and autophagy. It is noteworthy that **3y** was relatively nontoxic to human normal cells. Combination of **3y** with curcumin, an active, naturally occurring anti-cancer compound found in turmeric, a common ingredient in curry [96,97], increased **3y**-induced cytotoxicity on HCC cells. Using gene expression signatures of **3y** to query the C-Map, a small molecule, AR-A014418, an inhibitor of glycogen synthase kinase-3 (GSK-3) [98], was predicted to act similarly to **3y**. Further experiments confirmed that **3y** exhibited a cytotoxic effect by the induction of autophagy, and **3y** also behaved like AR-A014418 to suppress expression of phospho-GSK-3β.

2. Results and discussion

2.1. Design and synthesis of compounds

More recently, we reported a simple and facile protocol for the synthesis of 2*H*-1,4-benzoxazin-3(4*H*)-ones and their derivatives [99]. Owing to the biological importance of 1,2,3-triazoles and 2*H*-1,4-benzoxazin-3(4*H*)-ones scaffolds, we were primarily interested in the synthesis of 4-((1-benzyl-1*H*-1,2,3-triazol-4-yl)methyl)-2*H*-benzo[*b*] [1,4] oxazin-3(4*H*)-one (**3a**) from 4-(prop-2-ynyl)-2*H*-benzo[*b*] [1,4]oxazin-3(4*H*)-one (alkyne **1a**) and benzylazide via 1,3-dipolar cycloaddition in the presence of suitable metal catalysts. First, we performed a model reaction between alkyne **1a** with benzyl azide in the presence of CuI (0.3 equiv) in 1,4-dioxane at room temperature for 13 h leading to the formation of 4-((1-benzyl-1*H*-1,2,3-triazol-4-yl)methyl)-2*H*-benzo[*b*] [1,4]oxazin-3(4*H*)-one (**3a**) in 93% yield (Table 1, entry 1). Next, we investigated the effect of solvents on the formation of 4-((1-benzyl-1*H*-1,2,3-triazol-4-yl)methyl)-2*H*-benzo[*b*] [1,4]oxazin-3(4*H*)-one. Later performing the reactions in dimethyl sulfoxide (DMSO), DMF as solvents at room temperature produced 73% and 69% low product yields with several unidentified side products, respectively (Table 1, entries 2 and 3). We conducted same reaction in the absence of copper catalyst in DMSO at 100 °C for 24 h, the reaction did not lead to the formation of the required product (**3a**), and therefore we recovered the starting materials (Table 1, entry 4). Next we

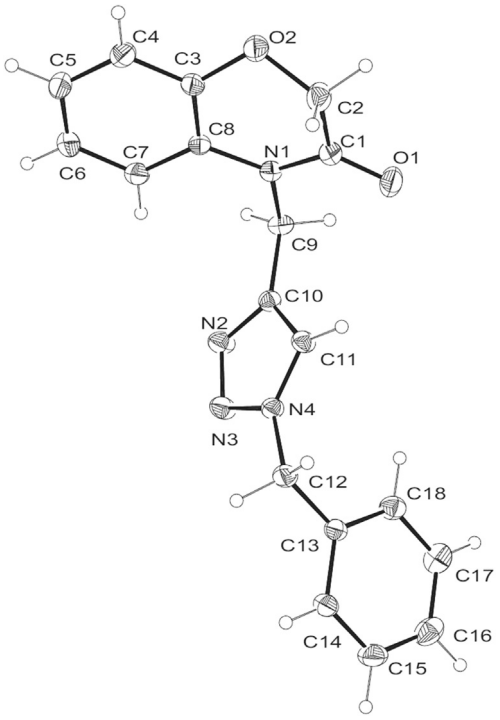

Fig. 1. Crystal structure of compound (**3a**) [103].

conducted the reactions in MeCN, THF furnished the moderate product yields (Table 1, entries 5 and 6). Employing the similar reaction conditions in toluene at 80 °C afforded moderate product yield (Table 1, entry 7). With protic solvents such as EtOH, H_2O under the same reaction conditions at 80 °C also produced moderate product yield (Table 1, entries 8 and 9). We performed the reaction under neat reaction condition at 80 °C furnished the low product yield (Table 1, entry 10). Applying the similar reaction conditions in 1,4-dioxane at 80 °C afforded the excellent product yield (Table 1, entry 11). The CuI catalyzed 1,3-dipolar cycloaddition reaction in 1,4-dioxane at 80 °C improved the product yields as well as reduced the reaction time. The results are summarized in Table 1. The starting materials including alkynes and azides were prepared according to previously reported procedure [100–102].

We next investigated the effect of the various copper catalysts on the formation of triazole (**3a**). Among the copper catalysts that we tested, CuI afforded the excellent product yield (Table 2, entry 11). The reaction did not lead to the formation of the required product (**3a**) in the absence of copper catalyst (Table 2, entry 1). With $CuSO_4 5H_2O$, very trace amount of desired product **3a** was

Table 4
Scope of the reaction with respect to azide.[a,b,c]

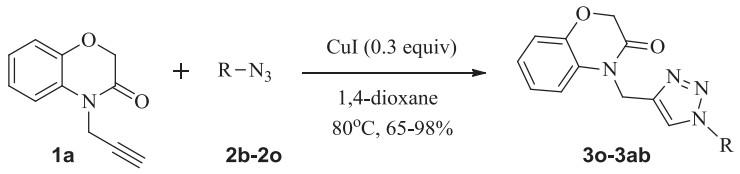

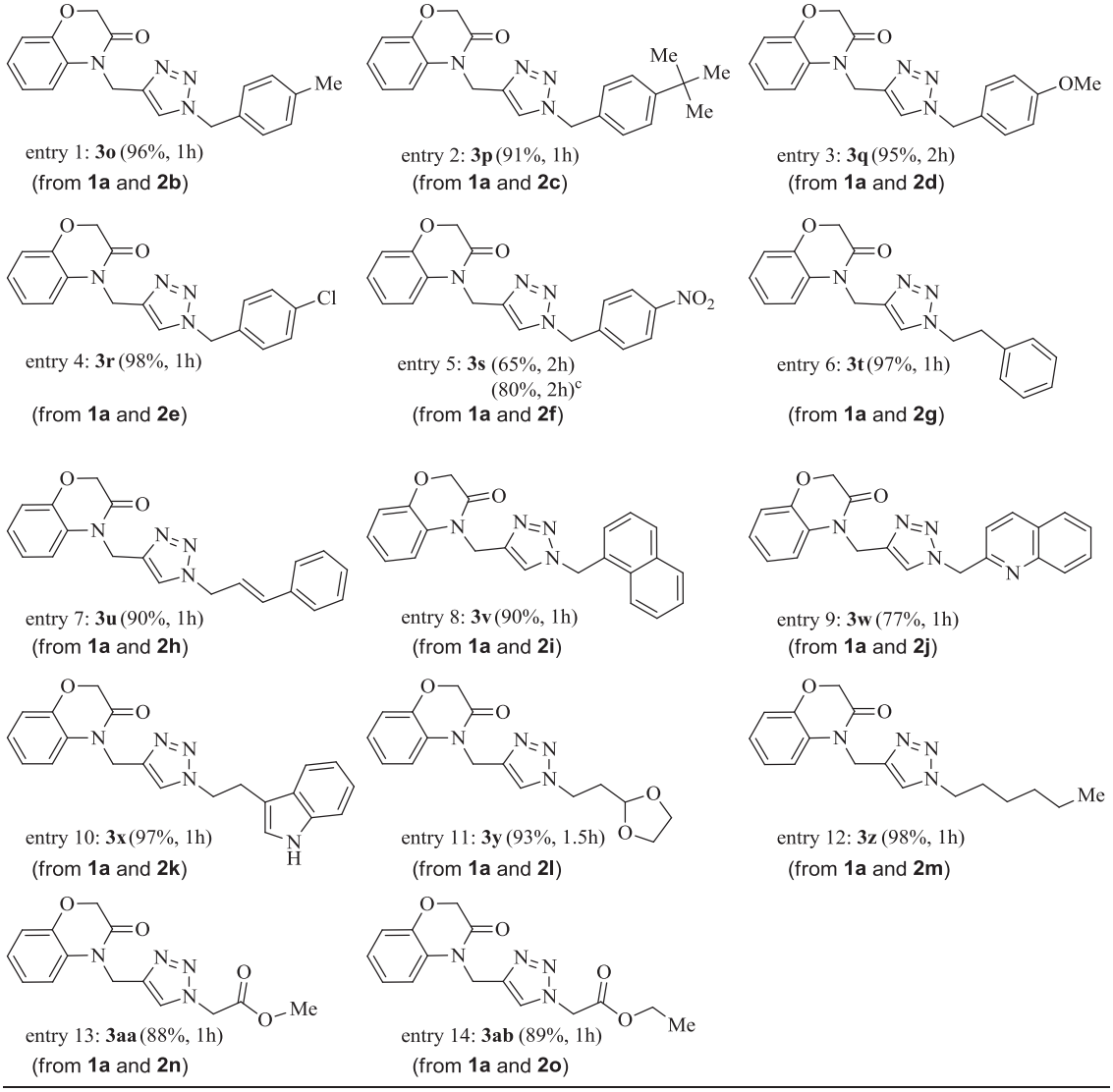

[a] All the reactions were carried out on 1 mmole scale.
[b] Isolated yields.
[c] Reaction in the presence of DIPEA.

isolated (Table 2, entry 2). Employing the similar reaction conditions with $Cu(OAc)_2$, $Cu(acac)_2$ catalysts were also effective and afforded good yields (Table 2, entries 3 and 4). Other copper catalysts such as CuBr, CuCl furnished the moderate product yields (Table 2, entries 5 and 6). We next investigated the amount of CuI required to catalyze the transformation. As little as 0.05 equivalent of CuI under the similar reaction conditions afforded the required product (**3a**) in 91% yield after 3.5 h (Table 2, entry 7). By means of 0.1 equivalent of CuI the product yield was afforded 92% yield after 3 h (Table 2, entry 8). Applying the similar reaction conditions with 0.15 equivalents of CuI produced the desired product (**3a**) in 92% yield after 2.5 h (Table 2, entry 9). Employing the similar reaction conditions with 0.2 equivalent of CuI afforded (**3a**) in 93% yield after 1.5 h (Table 2, entry 10). On the other hand, using 0.3 equivalent of CuI as a catalyst afforded the required product in 97% yield in 45 min (Table 2, entry 11). We observed some dependence on the amount of CuI used, with good improvement (reaction running time is decreased) upon increasing the catalyst loading to 0.3 equivalents. Hence, the optimum conditions involved in a reaction using alkyne (1.0 equiv) and azide (1.2 equiv) with CuI (0.3 equiv) in 1,4 dioxane (3.0 mL) as solvent heating at 80 °C. The results are summarized in Table 2.

With the optimized reaction condition in our hand, we performed the reactions with various substituted alkyne **1a** (Table 3). As shown in Table 3, benzyl azide treated with various substituted alkyne **1a** (Table 3, entries 1–14) to furnish the corresponding 1,4 disubstituted 1,2,3-triazole analogues containing 2*H*-1,4-benzoxazin-3-(4*H*)-one derivatives (**3a-3n**) in moderate to excellent product yields. The results were summarized in Table 3. The methyl substituent containing compounds underwent smooth reaction and produced excellent product yields (Table 3, entries 2 and 6). The halo substituent containing compounds well tolerated and afforded excellent product yields (Table 3, entries 3, 7 and 8). The electron donating groups like methoxy substituent containing compounds furnished the good product yield (Table 3, entries 4 and 9). The electron withdrawing group like ester substituent containing compound furnished the good product yield (Table 3, entry 10). The methyl and halo substituent containing compounds produced good product yield (Table 3, entry 5). The alkyl and aryl substituted compounds underwent longer running reaction of 3 h, but afforded good product yields (Table 3, entries 11, 12 and 13). Particularly noteworthy is that the 4-(prop-2-ynyl)-2*H*-pyrido[3,2-*b*] [1,4]oxazin-3(4*H*)-one afforded low product yield (Table 3, entry 14). All the 1,4-disubstituted 1,2,3-triazole analogues containing 2*H*-1,4-benzoxazin-3(4*H*)-one derivatives (**3a-3n**) obtained were fully characterized by the spectral techniques IR, ^{1}H, ^{13}C NMR and HRMS. The crystal structure of compound **(3a)** was shown in Fig. 1.

To further explore the generality and scope of this methodology, a range of azides were investigated (Table 4). All the azides were smoothly reacted with alkyne under the optimized reaction condition and afforded its required product (**3o-3ab**) in moderate to excellent yields, as single regioisomer (Table 4, entries 1–14). The moderately electron donating substituents like methyl and tertiarybutyl groups at para position containing benzyl azides furnished 96% and 91% product yields, respectively (Table 4, entries 2 and 5). The strong electron donating group like methoxy at para position containing benzyl azides afforded excellent product yield (Table 4, entry 3). The chloro substituent at para position containing benzyl azide produced in good yield (Table 4, entry 4). It is particularly noteworthy is that strong electron withdrawing groups like nitro at para position containing benzyl azide afforded moderate product yield (Table 4, entry 5). Employing the similar reaction conditions, the aryl azides such as (2-azidoethyl)benzene, (*E*)-(3-azidoprop-1-enyl)benzene and 1-(azidomethyl)naphthalene were smoothly reacted with alkyne **1a** and furnished the its corresponding products 97%, 90% and 91% yields, respectively (Table 4, entries 6, 7 and 8). The quinoline nucleus containing azide was under went smooth reaction with alkyne **1a** and it produced desired product in moderate yield (Table 4, entry 9). Whereas indole nucleus containing azide was well tolerated under the similar reaction conditions with alkyne **1a** and furnished its corresponding product in excellent yield (Table 4, entry 10). Applying the similar reaction conditions between 2-(2-azidoethyl)-1,3-dioxolane with alkyne **1a** the reaction was proceeded smoothly and afforded its corresponding product in good yield (Table 4, entry 11). This successful results were prompted us to extend the scope towards different aliphatic azides such as 1-azidohexane, methyl 2-azidoacetate and ethyl 2-azidoacetate were reacted smoothly with alkyne **1a** and furnished its desired products in excellent yields (Table 4, entries 12, 13 and 14). The results are summarized in Table 4. All the 1,4 disubstituted 1,2,3-triazoles analogues containing 2*H*-1,4-benzoxazin-3(4*H*)-one derivatives (**3o-3ab**)

Table 5
The IC_{50} of the synthetic novel compounds listed in Table 3 on human cancer cells.

	Hep 3B (μM)	HT-29 (μM)
3a	84.5	>100
3b	>100	54.9
3c	0.9	>100
3d	9.2	9.3
3e	>100	19.6
3f	>100	>100
3g	55.5	76.5
3h	>100	>100
3i	>100	>100
3j	17.1	41.5
3k	>100	>100
3l	61.8	>100
3m	>100	>100
3n	8,7	12.8

Human HCC Hep 3B cells and human colorectal cancer HT-29 cells were treated with 0, 5, 10 μM of the indicated compound for 6 days. A concentration of 10 μM was used because, in general, the IC_{50} should be less than 10 μM for further clinical application. Growth inhibition was evaluated by MTT assay. The values of IC_{50} were calculated by interpolation and extrapolation. Results were representative of three independent experiments. Oxaliplatin, a FDA-approved anti-cancer drug, was used as a positive control, and the IC_{50} values on Hep 3B and HT-29 were determined to be 3.3 and 3.4 μM.

Table 6
The IC_{50} of the synthetic novel compounds listed in Table 4 on human cancer cells.

	Hep 3B (μM)	HT-29 (μM)
3aa	>100	50.8
3ab	19.0	36.4
3o	>100	28.6
3p	25.6	25.1
3q	>100	18.5
3r	>100	21.9
3s	29.6	15.6
3t	66.0	48.8
3u	38.9	>100
3v	15.2	17.0
3w	>100	>100
3x	70.0	15.2
3y	0.5	5.7
3z	>100	34.4

Human HCC Hep 3B cells and human colorectal cancer HT-29 cells were treated with 0, 5, 10 μM of the indicated compound for 6 days. A concentration of 10 μM was used because, in general, the IC_{50} should be less than 10 μM for further clinical application. Growth inhibition was evaluated by MTT assay. The values of IC_{50} were calculated by interpolation and extrapolation. Results were representative of three independent experiments. Oxaliplatin, a FDA-approved anti-cancer drug, was used as a positive control, and the IC_{50} values on Hep 3B and HT-29 were determined to be 3.3 and 3.4 μM.

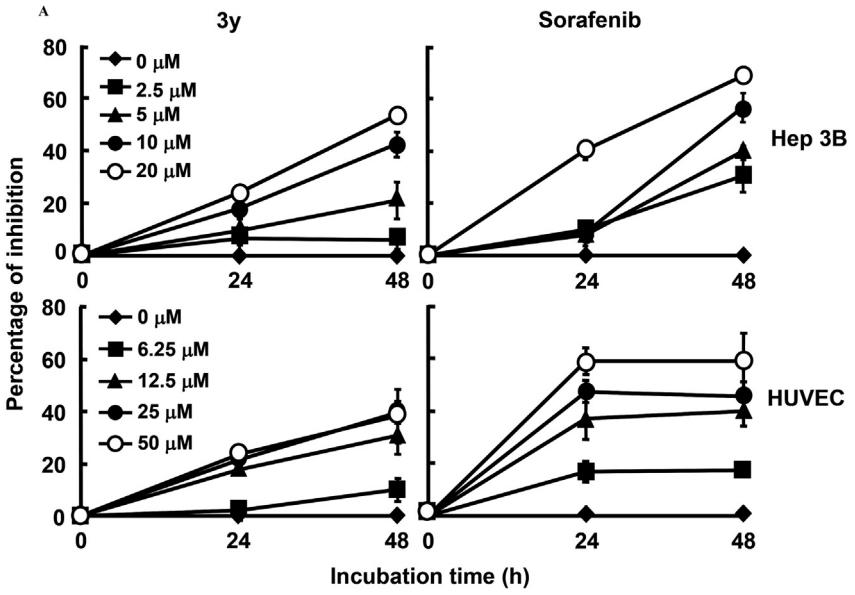

	Hep 3B	HUVEC
	IC_{50} (μM)	
3y	16.8 ± 0.9[b]	115.0 ± 16.9[a]
Sorafenib	11.2 ± 0.6[b]	40.6 ± 13.0[b]

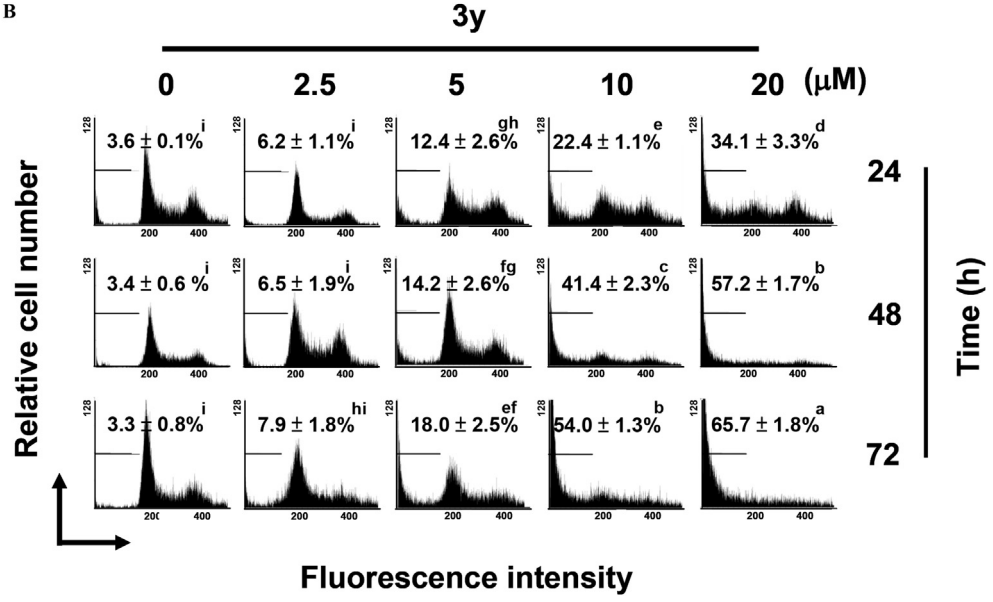

Fig. 2. The cytotoxic effects of **3y** and Sorafenib. (A) Cytotoxicity of **3y** and Sorafenib on human cancer and normal cells. After treatment, growth inhibition was evaluated by MTT assay. Data from at least three independent experiments at 48 h were used to calculate IC_{50}. The IC_{50} for **3y** in HUVEC cells was extrapolated. The data were expressed as means ± SEMs. Means in the same cell type without a common letter differ, $P < 0.05$. (B) **3y** induced apoptosis of Hep 3B cells in a time- and dose-related manner. (C) Sorafenib-induced apoptosis of Hep 3B cells was only observed at a higher concentration for a longer period of time. After treatment, Hep 3B cells were stained with PI before flow cytometry. The percentages in the figure indicate the percentages of apoptotic cells. The percentages of cells at different phases of cell cycle were also determined. The data were analyzed by one-way ANOVA. Differences among groups were analyzed by Duncan's multiple range tests. Means in each cell cycle without a common letter differ, $P < 0.05$. (D) **3y** induced autophagy of Hep 3B cells in a time- and dose-related manner. (E) Sorafenib-induced autophagy of Hep 3B cells was only observed at a higher dosage for a longer period of time. After treatment, Hep 3B cells were stained with AO before flow cytometry. The percentages in the figure indicate the proportion of cells (upper two quadrants) with AVOs staining. Data are presented as means ± SEMs. The data were analyzed by one-way ANOVA. Differences among groups were analyzed by Duncan's multiple range tests. Means without a common letter differ, $P < 0.05$. Results are representative of three independent experiments.

C

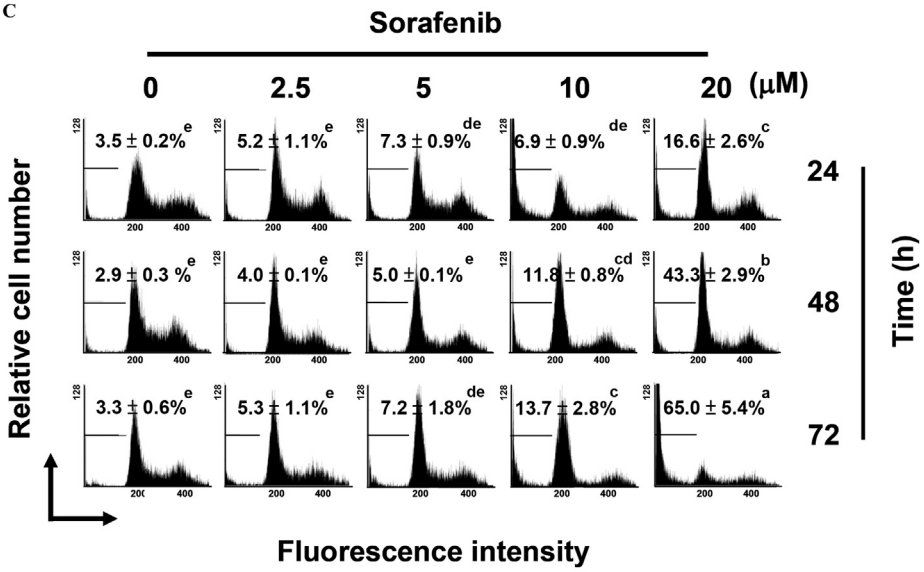

Time (h)	24				
Sorafenib (μM)	0	2.5	5	10	20
			%		
Sub-G1	3.5±0.2^{e}	5.2±0.4^{e}	7.3±0.9^{de}	6.9±0.9^{de}	16.6±2.6^{c}
G0/G1	39.0±0.4^{c}	38.1±1.5^{c}	38.1±2.5^{c}	53.6±1.7^{ab}	45.7±4.1^{bc}
S	22.6±1.6^{a}	21.9±0.9^{a}	19.8±0.7^{ab}	12.3±3.2^{cde}	14.3±1.1^{c}
G2/M	34.9±2.0^{ab}	35.1±2.0^{ab}	34.9±3.5^{ab}	27.2±2.9^{bcd}	23.5±2.9^{cde}
Time (h)			48		
Sub-G1	2.9±0.3^{e}	4.0±0.1^{e}	0.5±0.1^{e}	11.8±0.8^{cd}	43.3±2.9^{b}
G0/G1	40.4±0.3^{c}	44.1±2.5^{c}	42.3±2.9^{c}	54.9±3.9^{a}	27.8±2.1^{d}
S	20.8±1.3^{a}	16.2±1.4^{bc}	13.1±1.1^{cd}	8.8±1.0^{ef}	9.6±0.9^{def}
G2/M	35.9±2.0^{ab}	35.7±2.8^{ab}	39.6±3.2^{a}	24.5±4.0^{cde}	19.2±2.8^{b}
Time (h)			72		
Sub-G1	3.3±0.6^{e}	5.3±1.1^{e}	7.2±1.8^{de}	13.7±2.8^{c}	65.0±5.4^{a}
G0/G1	41.6±2.0^{c}	43.8±1.9^{c}	47.8±2.3^{abc}	55.7±3.5^{a}	13.6±1.7^{e}
S	16.4±1.0^{bc}	15.0±1.0^{c}	13.7±0.5^{cd}	7.9±1.4^{f}	6.2±1.2^{f}
G2/M	28.7±2.6^{a}	35.9±2.4^{ab}	31.3±3.5^{abc}	22.7±2.1^{cde}	15.2±4.2^{e}

D

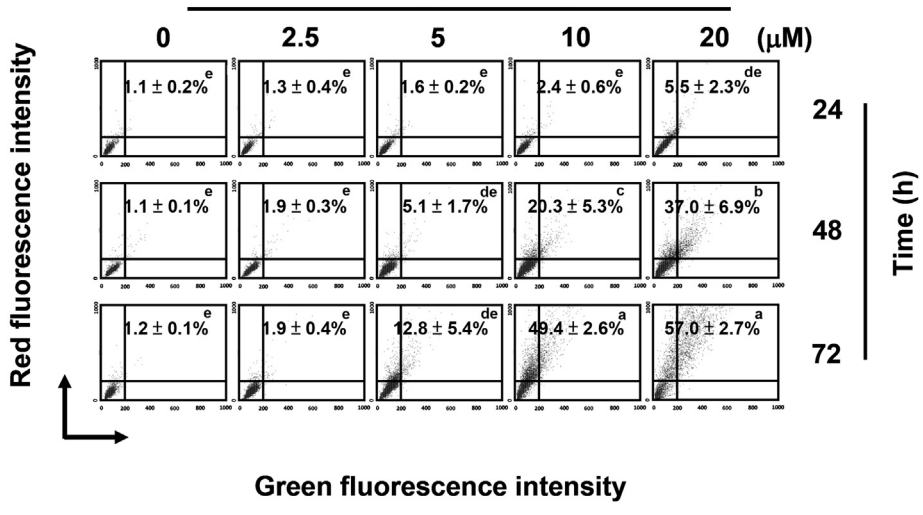

Fig. 2. (*continued*).

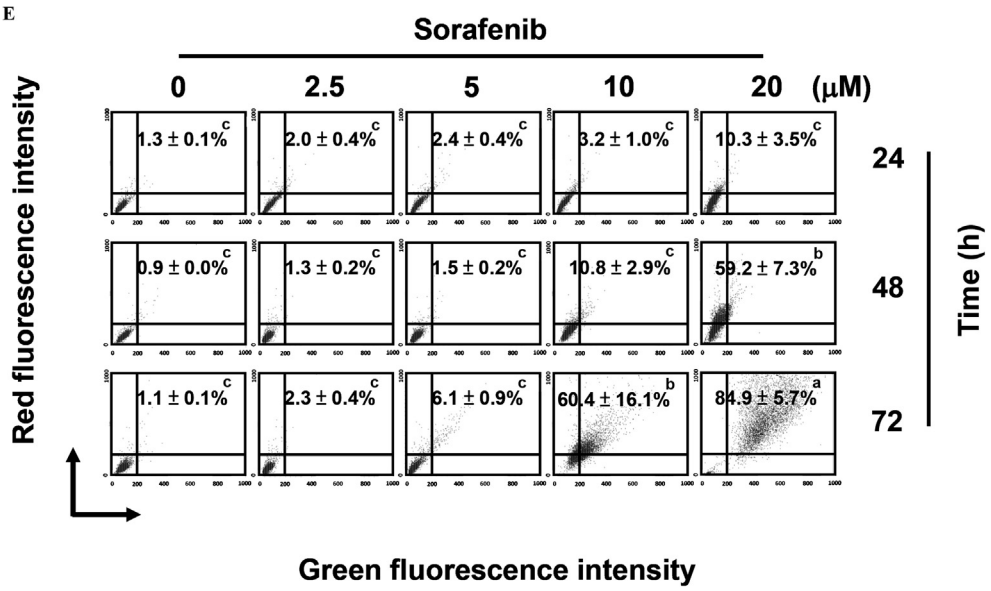

Fig. 2. (*continued*).

obtained were fully characterized by the spectral techniques IR, ^{1}H, ^{13}C NMR and HRMS.

2.2. Growth inhibition of human cancer cells by the novel synthetic compounds

To examine if these newly synthetic compounds exhibit anticancer effect, the growth of human HCC Hep 3B and human colorectal cancer HT-29 cells in the presence of these compounds was determined and the 50% inhibitory concentration (IC_{50}) was calculated. The Hep 3B cell line (American Type Culture Collection, Rockville, MD) contains an integrated hepatitis B virus genome and expresses hepatitis B surface antigen, as well as expresses mutated p53, one of most frequently mutated gene in HCC. The HT-29 cell line is apoptosis-resistant to 5-fluorouracil/leucovorin or oxaliplatin due to fully functional stat6 signaling and the lack of a functional pro-apoptotic p53.

First, we tested the compounds in Table 3 using 3-[4,5-Dimethylthiazol-2-yl]-2,5-diphenyltetrazolium bromide (MTT) assay. Compounds with a variety of substituents connected to 2*H*-1,4-benzoxazin-3-(4*H*)-one exhibited varies toxicity on Hep 3B and HT-29 cancer cells (Table 5). Among these compounds, **3d** with methoxyl group connected to 2*H*-1,4-benzoxazin-3-(4*H*)-one showed high potency in inhibiting cell growth. Due to the solubility of **3a**, the inhibition of cell growth is less than **3d**. However, the high yield of synthetic step and feasible purification drive us to modify **3a** by connecting a variety of azide groups.

The compound structures shown in Table 4 and IC_{50} with Hep 3B and HT-29 are listed in Table 6. Among these compounds, **3y** displayed the lowest value of IC_{50} for both cancer cell lines, suggesting that **3y** exhibited the best cytotoxic effect. It is noteworthy that Hep 3B cells were more sensitive to **3y** compared to HT-29 cells. Therefore, Hep 3B cells were used in the following experiments to determine the cytotoxic mechanism of **3y**.

2.3. 3y exhibited better cytotoxic effect than sorafenib when HCC Hep 3B cells were treated at a lower concentration for a shorter period of time

To determine the chemotherapeutic potential of **3y** on HCC, Hep 3B cells were treated with **3y** or Sorafenib, the only FDA-approved targeted therapy for HCC. As shown in Fig. 2A, the growth of Hep 3B cells was inhibited by **3y** and Sorafenib separately in a time- and dosage-dependent manner. At a concentration of 20 μM, Sorafenib exhibited a better cytotoxic effect (40.2 and 68.4%, respectively) than that of **3y** (24.1 and 53.4%, respectively) at 24 and 48 h. However, 10 μM **3y** exhibited a higher percentage of growth inhibition (18.0%) than that of Sorafenib (8.6%) at 24 h, suggesting that **3y**, at a lower concentration and for a shorter period of time, displayed a better cytotoxic effect than that of Sorafenib. To insure the sustaining effect of the compounds, cells were treated for 6 days (Table 6). Since the standard treatment of Sorafenib is 400 mg, twice a day [104], The better cytotoxic effect of **3y** than Sorafenib at the early time points suggested the application of **3y**.

2.4. 3y displayed lower cytotoxicity on human normal cells

To compare the side effects of **3y** with those of Sorafenib, normal human umbilical vein endothelial cells (HUVEC) were used. As shown in Fig. 2A, at a time point of 24 h, 12.5, 25, and 50 μM Sorafenib induced growth inhibition rates of 37.4, 41.4, and 60.0% on HUVEC, which were higher (15.2, 23.8, and 21.5%, respectively) than those of **3y**. For a longer period of time (48 h), treatment of HUVEC with Sorafenib (12.5, 25, and 50 μM) also exhibited a stronger inhibition effect on HUVEC compared with that of **3y**. To determine the cytotoxicity of **3y** and Sorafenib separately on human cancer and normal cells, the IC_{50} for Hep 3B and HUVEC were calculated and extrapolated, respectively (Fig. 2A). It is noteworthy that the IC_{50} of **3y** for Hep 3B cells was similar to that of Sorafenib, and that of **3y** for normal HUVEC was significantly higher ($P < 0.05$) than that of Sorafenib, suggesting that **3y** has milder side effects than those of Sorafenib.

2.5. 3y induced apoptosis of Hep 3B cells

Apoptosis (programmed cell death type I) has attracted considerable attention in cancer therapy research as the induction of apoptosis has been shown to be a potentially promising approach for cancer treatment [105]. Apoptotic signaling cascades ultimately lead to fragmentation of DNA [105] and formation of

apoptotic bodies [106], and therefore apoptotic cells with reduced DNA content produce a peak at the sub-G1 position [107]. The inhibition of cell growth using MTT assay (Fig. 2A) may result from the induction of cell death and/or suppression of cell proliferation. In order to understand the possible mechanisms of **3y**-induced cytotoxicity on HCC, phases of the cell cycle, including the sub-G1 phase of Hep 3B cells, were determined using propidium iodide (PI) staining before flow cytometry. The anti-cancer drug Sorafenib was used as a positive control. As shown in Fig. 2B, **3y** increased the percentages of Hep 3B cells at the sub-G1 phase, representing apoptosis [107], in a time-related manner. Ten μM **3y** significantly ($P < 0.05$) increased the apoptotic rates from 22.4% at 24 h to 41.4% and 54.0% at 48 h and 72 h, respectively. Significant ($P < 0.05$) elevations in the percentages of apoptotic cells from 34.1% at 24 h to 57.2% and 65.7% at 48 h and 72 h were also observed when Hep 3B cells were treated with 20 μM **3y**. Dose-related increases in apoptosis by **3y** were found in Hep 3B cells, ranging from 3.6% in non-treated cells to 12.4, 22.2, and 34.1% in those treated with 5, 10, and 20 μM **3y** for 24 h, respectively. Dose-dependent increases in the cells at the sub-G1 phases were also observed when Hep 3B cells were treated with **3y** for 48 and 72 h. The distributions of the cell cycle phases indicate that **3y** only induced apoptosis of Hep 3B cells and did not cause cell cycle arrest at the G0/G1, S, or G2/M phases. The decrease in percentages of cells at G0/G1, S, and G2/M may have been due to the increase of cells at the Sub-G1 phase.

Sorafenib also induced apoptosis of Hep 3B cells in a time- and dose-related manner (Fig. 2C). However, significant increases were only observed when Hep 3B cells were treated with 10 μM Sorafenib for 48–72 h or with 20 μM Sorafenib for 24–72 h. Although the treatment of Hep 3B cells with 20 μM of **3y** (65.7%) or Sorafenib (65.0%) for 72 h resulted in similar percentages of cells at the sub-G1 phase, treatments of **3y** either at a lower concentration or for a shorter period of time led to greater increases in apoptotic rates compared with those treated with Sorafenib under corresponding conditions. The mean plasma concentration of sorafenib in HCC patients receiving a standard treatment with sorafenib (400 mg, twice a day) is about 10 μM [104]. The greater elevation in apoptosis in response to 10 μM of **3y** than Sorafenib, suggesting **3y** may be a better apoptosis inducer.

2.6. *3y triggered autophagy of Hep 3B cells*

Recent research indicates that autophagy (programmed cell death type II) and apoptosis may be interconnected in the determination of a cell's fate. To examine whether **3y** is able to induce autophagy in HCC cells, Hep 3B cells were stained with acridine orange (AO) before flow cytometry. As shown in Fig. 2D, **3y** induced autophagy of Hep 3B cells in a time-related manner. At a concentration of 10 μM, **3y** increased the percentages of cells undergoing autophagy from 2.4% at 24 h to 20.3% and 49.4% at 48 h and 72 h, respectively. At a concentration of 20 μM, **3y** elevated the percentages of autophagic cells from 5.5% at 24 h to 37.0% and 57.0% at 48 h and 72 h, respectively. Dose-related induction of autophagy by **3y** was also observed in Hep 3B cells, except for the time point at 24 h. At 48 h, **3y** induced autophagy in a dose-related manner, ranging from 1.1% in non-treated cells to 5.1, 20.3, and 37.0% in those treated with 5, 10, and 20 μM **3y**, respectively. Dose-related elevation in autophagy by **3y** was also observed in Hep 3B cells at 72 h.

Sorafenib also induced autophagy of Hep 3B cells in a time- and dose-related manner (Fig. 2E). Although Sorafenib-induced autophagy was greater than **3y,** especially at a higher concentration (10 μM for 72 h and 20 μM for 24–72 h), it is noteworthy that the lower concentrations of **3y** (5–10 μM for 48 h and 5 μM for 72 h) seemed to induce a greater percentage of autophagy compared

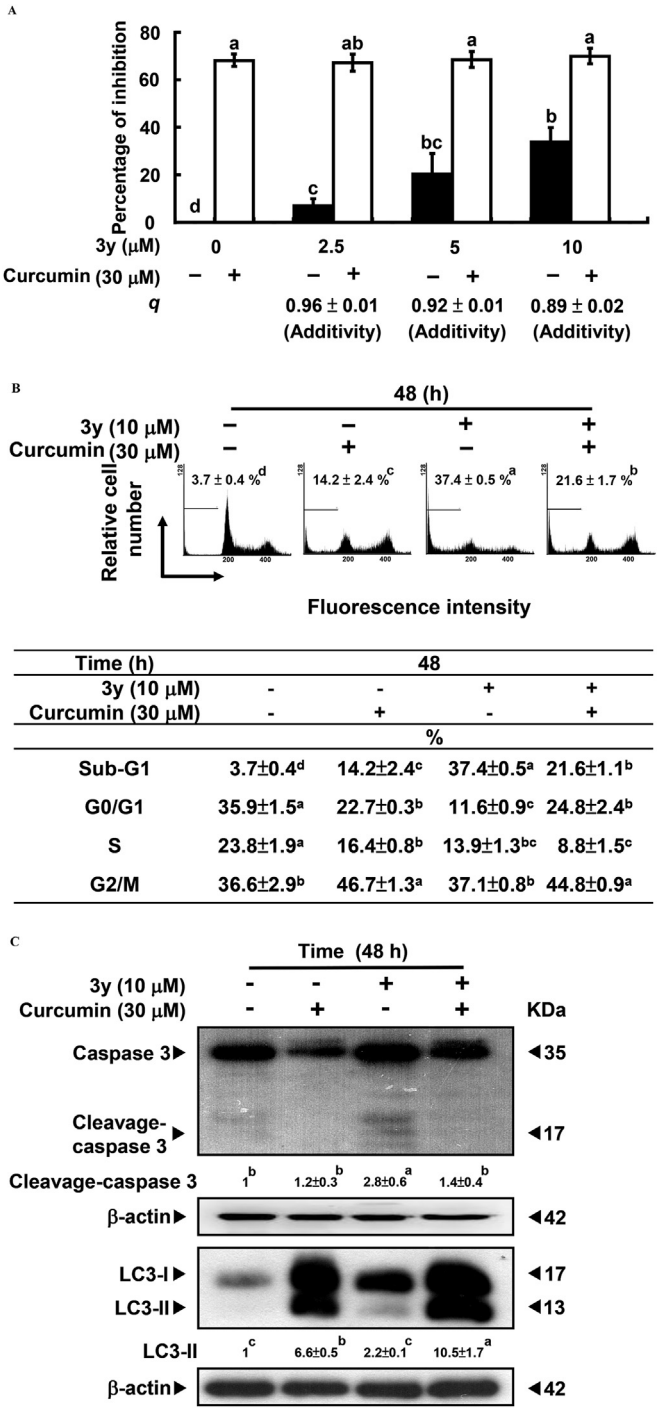

Time (h)	48			
3y (10 μM)	-	-	+	+
Curcumin (30 μM)	-	+	-	+
	%			
Sub-G1	3.7±0.4^{d}	14.2±2.4^{c}	37.4±0.5^{a}	21.6±1.1^{b}
G0/G1	35.9±1.5^{a}	22.7±0.3^{b}	11.6±0.9^{c}	24.8±2.4^{b}
S	23.8±1.9^{a}	16.4±0.8^{b}	13.9±1.3^{bc}	8.8±1.5^{c}
G2/M	36.6±2.9^{b}	46.7±1.3^{a}	37.1±0.8^{b}	44.8±0.9^{a}

Fig. 3. The combination effect of **3y** and curcumin. (A) Curcumin enhanced cytotoxicity of **3y**. Human HCC Hep 3B cells were treated with **3y** with or without curcumin for 48 h. Growth inhibition was evaluated by MTT assay. The data are expressed as means ± SEMs. Means without a common letter differ, $P < 0.05$. Data from at least three independent experiments were used to calculate the interaction (q value) of **3y** and curcumin. (B) Curcumin did not promote **3y**-induced apoptosis using flow cytometry. After treatment, Hep 3B cells were stained with PI before flow cytometry. The percentages in the figure indicate the percentages of apoptotic cells. The percentages of cells at different phases of cell cycle were also determined. Means in each cell cycle without a common letter differ, $P < 0.05$. (C) Curcumin increased autophagy marker LC3-II expression in **3y**-treated cells. After treatment, whole cell lysates were subjected to Western blot analysis. Anti-caspase 3 and anti-LC3 antibodies served as probes. β-actin served as a loading control. The intensity of each protein expression band of at least three independent experiments was quantified by densitometry normalizing to that of β-actin, with control level arbitrarily set to 1. Data are presented as means ± SEMs. Means in each protein without a common letter differ, $P < 0.05$. Results are representative of three independent experiments.

with Sorafenib under the same experimental conditions.

Although **3y** appears to be marginally better than Sorafenib (Fig. 2), lower cytotoxicity of **3y** on normal human cells suggested the application of **3y**. The adverse effects of Sorafenib include increases in the risk of hypertension, bleeding, and arterial thromboembolism [83–86], reducing patients' quality of life.

2.7. Curcumin-enhanced cytotoxic effect of 3y by further induction of autophagy, not apoptosis

Curcumin, an active, naturally occurring compound present in turmeric, is a safe and readily available food ingredient worldwide which has been shown to have chemopreventive and chemotherapeutic potential in human cancers [108]. Recently, curcumin-induced enhancement in anti-tumor activity and reduction in adverse reactions of doxorubicin, the FDA-approved anti-cancer drugs used routinely as a single drug for advanced HCC, has been reported [109]. **3y** exhibited significant cytotoxicity on Hep 3B cells (Figs. 1–2), suggesting the anti-cancer potential of **3y** for HCC. The experiments were carried out to determine if addition of curcumin altered the cytotoxic effect of **3y**. Hep 3B cells were incubated with **3y** with or without curcumin for 48 h, and MTT assay was performed to determine the cytotoxicity of the cells. As shown in Fig. 3A, **3y** alone induced growth inhibition of Hep 3B cells in a dose-related manner. Curcumin alone also significantly suppressed the growth of Hep 3B cells. It is noteworthy that combination of **3y** and curcumin significantly increased the cytotoxicity of **3y**. Although it produced an additivity effect (mean q ranges from 0.89 to 0.96), the cytotoxicity of the combination treatment was very similar to that of curcumin alone. To determine if induction of apoptosis and cell cycle arrest were involved in curcumin-enhanced cytotoxic activity of **3y**, the **3y**-induced increases in the percentage of cells at different cell cycles were examined. As shown in Fig. 3B, **3y** or curcumin alone induced apoptosis, and **3y** induced a significantly greater effect than that of curcumin. Addition of curcumin did not further increase **3y**-induced apoptosis. To confirm that the induction of apoptosis was not involved, expression of cleavage-caspase 3, representing the activation of extrinsic and/or intrinsic apoptotic pathways [110], was determined. As shown in Fig. 3C (upper panel), addition of curcumin did not increase **3y**-induced cleavage-caspase 3 expression, confirming that the induction of apoptosis was not involved in the curcumin-enhanced cytotoxicity. It is noteworthy that expression of autophagy marker LC3-II increased significantly ($P < 0.05$) when curcumin and **3y** were coadministrated compared with that achieved by curcumin or **3y** alone, suggesting that further induction of autophagy was involved in curcumin-enhanced cytotoxicity on HCC Hep 3B cells. In a previous study, the data revealed that autophagy is downregulated in human hepatitis B virus-associated HCC specimens, and that low level of autophagy occurs during hepatitis B virus-associated HCC development [111]. Induction of autophagy of Hep 3B cells (The cell line contains an integrated hepatitis B virus genome and expresses hepatitis B surface antigen; ATCC) in response to **3y** (Fig. 2D) and elevation of **3y**-induced autophagy by co-treatment of curcumin (Fig. 3C) suggest a new avenue for the treatment of HCC. Enhancement of cytotoxicity by addition of curcumin was also observed in HCC Hep G2 and lung adenocarcinoma A549 cells [112,113]. Curcumin, is a highly pleiotropic molecule which exhibits an anti-cancer effect *in vitro*, *in vivo*, and in human clinical trials [96,108,114]. Induction of tumor apoptosis, autophagy, and inhibition of tumor proliferation, invasion, angiogenesis, and metastasis are possible anti-cancer mechanisms of curcumin [115–117]. Since turmeric is an ingredient commonly used in the traditional diet of many Asian countries and is frequently used in Indian herbal medicine, the increase in anti-cancer activity by addition of curcumin suggests that the intake of foods rich in curcumin or curcumin-containing supplements may have a role to play in cancer prevention and therapy.

A

Hep-3B 1 μM > 3.0

Up-regulated	Down-regulated				
TSTA3	SLC27A3	DUSP11	EDN1	PTPRC	HIST2H2BE
ARFIP2	FOS	ORC1	ARL4C	GNA15	DNMT3A
RPS6KA1	PPP1R13B	PTPRK	PLA2G4A	MMP2	PIK3CA
CDCA4	HTRA1	UBE2J1	PPOX	ZNF586	EXT1
CCND1	FUT1	IL1B	NVL	CHAC1	FAM69A
OXA1L	SHB	PTK2B	TFAP2A	SNX13	GRB7
CDKN1A	PAPD7	TGFB3	PLEKHM1	SNX7	SUPV3L1
	CD40	FZD1	CTNND1 /// TMX2-CTNND1	RTN2	ARNT2

B

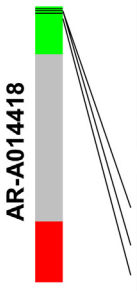

Rank	C-Map name	Mean	n	Enrichment	P	Specificity	% Non-null
1	AR-A014418	0.679	3	0.977	0.00004	0.0000	100
2	Procaine	-0.565	5	-0.834	0.00032	0.0000	100
3	Wortmannin	-0.371	18	-0.470	0.00042	0.1338	66
4	Harmol	0.628	4	0.858	0.00054	0.0155	100

Rank	Batch	C-Map name	Dose	Cell	Score
51	1077	AR-A014418	10 μM	PC3	0.713
89	1076	AR-A014418	10 μM	MCF-7	0.676
144	1071	AR-A014418	10 μM	PC3	0.647

Fig. 4. AR-A014418 might exhibit similar molecular action to **3y**. (A) Hep 3B cells were treated with 1 μM treatment of **3y** and then subjected to L1000 profiling. The gene signature was obtained from the fold change of the expression level set at log2 value as > 3.0 and < −3.0. (B) Using this gene signature to query C-Map, AR-A014418 (a GSK-3 inhibitor) was ranked as the top 1 drug with enrichment score of 0.977.

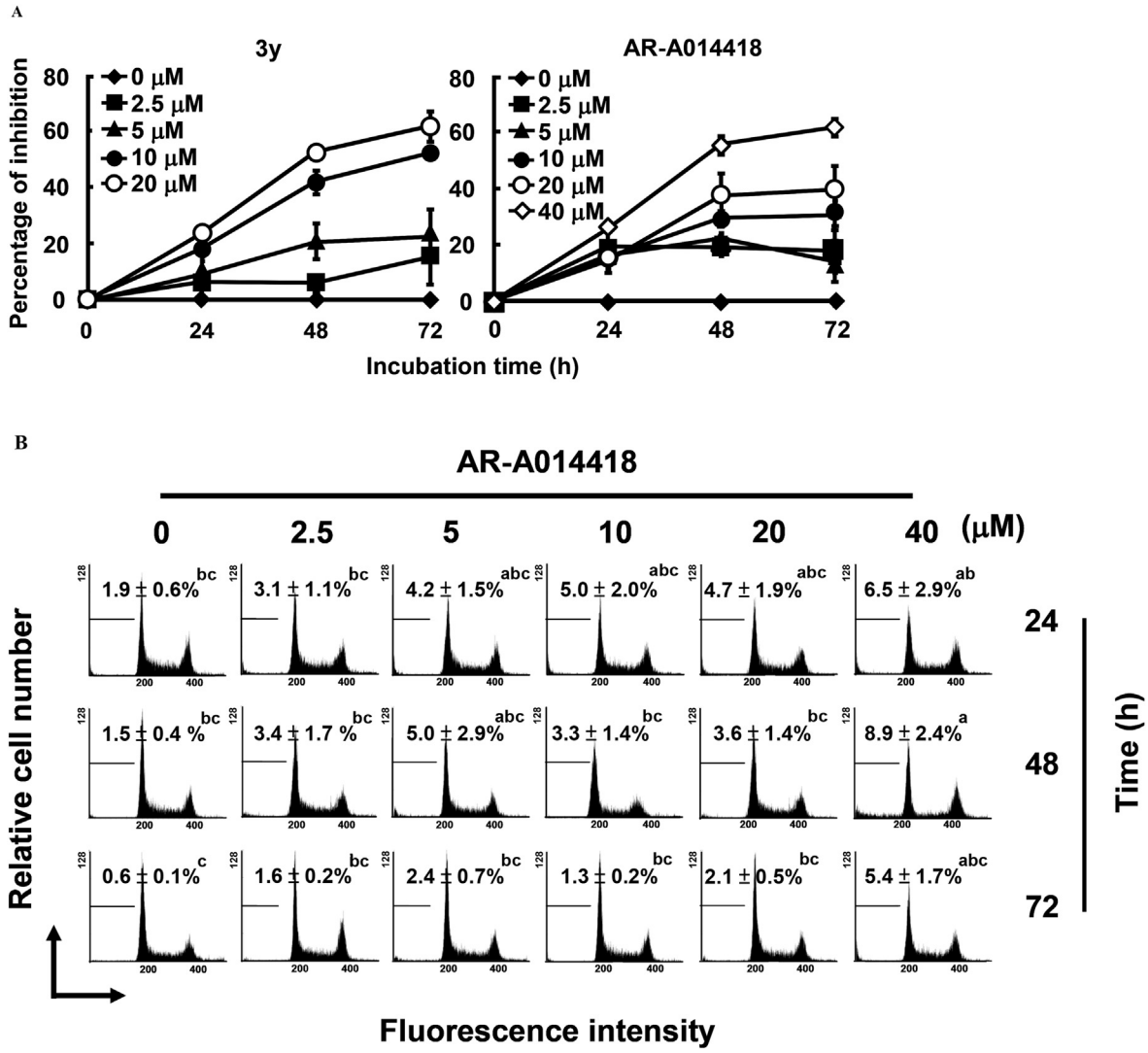

Time (h)	24					
AR-A014418 (μM)	0	2.5	5	10	20	40
	%					
Sub-G1	1.9±0.6^{bc}	3.1±1.1^{bc}	4.2±1.5^{a-c}	5.0±2.0^{a-c}	4.7±1.9^{a-c}	6.5±2.9^{ab}
G0/G1	36.3±0.9^{c-f}	36.8±0.8^{c-f}	32.5±2.6^{f}	34.3±2.1^{d-f}	33.0±1.9^{ef}	35.0±1.7^{d-f}
S	27.1±2.2^{a}	25.7±2.2^{ab}	25.0±2.2^{ab}	23.4±3.0^{ab}	25.1±3.5^{ab}	21.1±3.2^{a-c}
G2/M	31.8±1.5^{c}	34.7±2.0^{bc}	35.3±0.2^{bc}	38.5±3.1^{a-c}	37.6±3.5^{a-c}	37.6±1.1^{a-c}
Time (h)	48					
Sub-G1	1.5±0.4^{bc}	3.4±1.7^{bc}	5.0±2.9^{a-c}	3.3±1.4^{bc}	3.6±1.4^{bc}	8.9±2.4^{a}
G0/G1	39.7±0.4^{b-d}	38.5±2.1^{b-f}	38.5±1.1^{b-f}	39.4±2.5^{b-e}	37.8±0.5^{b-f}	34.7±3.0^{d-f}
S	24.0±2.0^{ab}	23.2±1.5^{ab}	24.6±1.0^{ab}	23.2±1.4^{ab}	20.0±1.8^{bc}	14.9±1.2^{cd}
G2/M	34.8±1.8^{bc}	34.9±1.6^{bc}	31.8±2.5^{c}	34.1±0.2^{c}	38.7±2.0^{a-c}	41.6±2.6^{ab}
Time (h)	72					
Sub-G1	0.6±0.1^{c}	1.6±0.2^{bc}	2.4±0.7^{bc}	1.3±0.7^{bc}	2.1±0.5^{bc}	5.4±1.7^{a-c}
G0/G1	46.2±1.7^{a}	42.3±2.5^{a-c}	42.4±1.0^{a-c}	43.3±1.9^{ab}	43.6±2.3^{ab}	38.5±2.6^{b-f}
S	21.1±0.3^{a-c}	21.1±1.4^{a-c}	21.7±1.9^{ab}	21.5±0.1^{ab}	19.5±0.9^{bc}	13.5±0.9^{d}
G2/M	32.3±1.8^{c}	35.3±2.7^{bc}	33.9±2.3^{c}	34.1±1.7^{c}	34.9±2.5^{bc}	42.8±2.57^{a}

Fig. 5. The similarity of **3y** and AR-A014418. (A) Cytotoxicity of **3y** and AR-A014418 on human HCC cells. After treatment, growth inhibition was evaluated by MTT assay. The data are expressed as means ± SEMs. (B) AR-A014418 did not induce apoptosis of Hep 3B cells. After treatment, Hep 3B cells were stained with PI before flow cytometry. The percentages in the figure indicate the percentages of apoptotic cells. The percentages of cells at different phases of cell cycle were also determined. Means in each cell cycle without a common

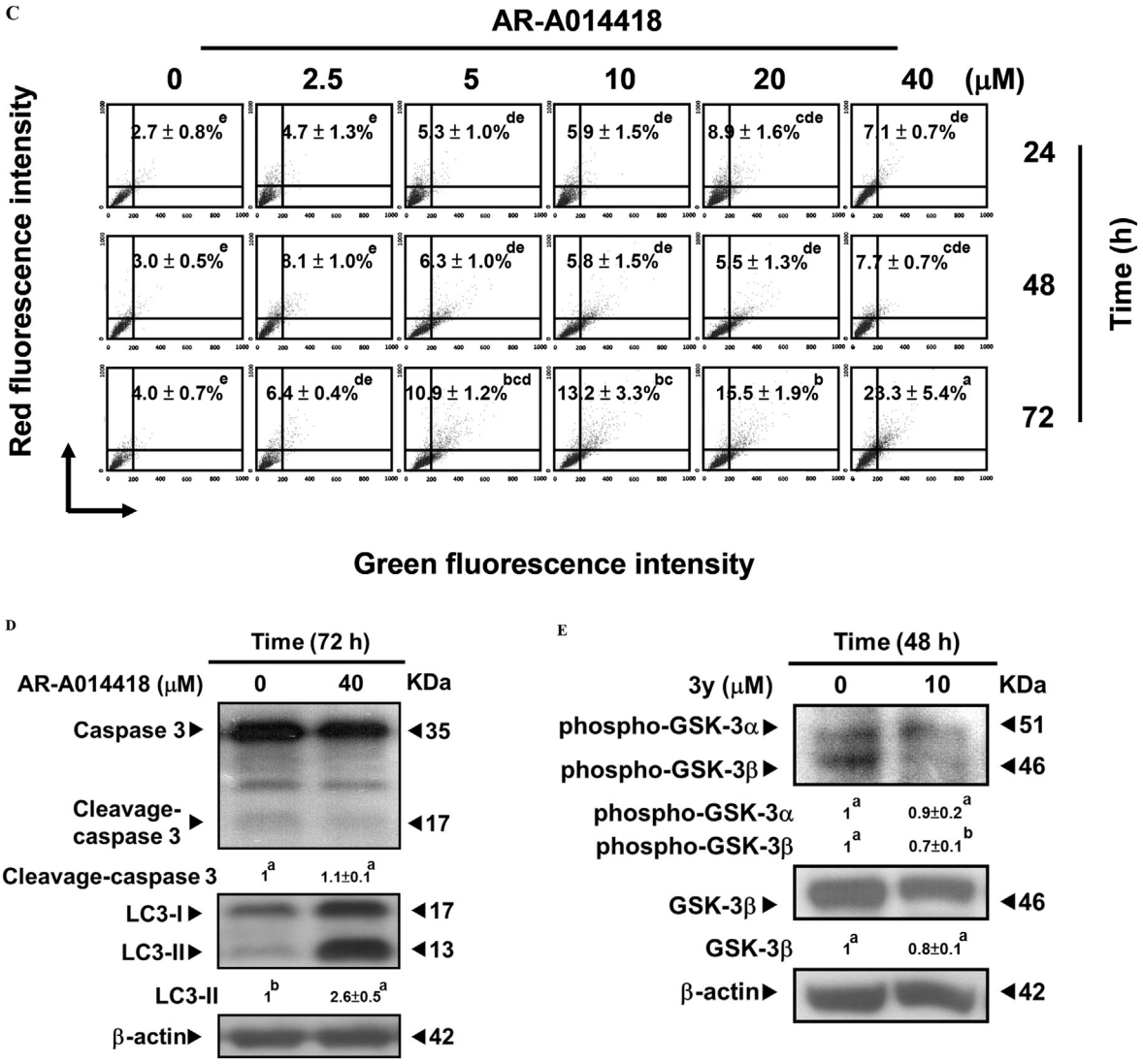

Fig. 5. (*continued*).

2.8. ***3y*** *behaved similarly to AR-A014418, and vice versa*

To elucidate other biological mechanisms of **3y**, the gene expression changes of Hep 3B cells induced by **3y** were obtained using the L1000 profiling platform. To obtain the predictive drug lists, both gene signatures from 1 μM to 10 μM treatments were employed to query C-Map respectively using the following 4 criteria: (1) the fold change of the expression level was set at log2 value as > 2.5 and < −2.5, (2) the fold change of the expression level was set at log2 value as > 3.0 and < −3.0, (3) top 10 of up- and down-regulated probe sets, and (4) top 20 of up- and down-regulated probe sets. Furthermore, we only selected drugs with enrichment score >0.5, and *P* value < 0.01 as candidates, and ranked the priority by their frequency from eight queries. Taken together, we found that AR-A014418 (an inhibitor of GSK-3) [98] might display similar molecular action to that of **3y**. One of the query results is shown in Fig. 4 and Supporting Information. To confirm this result, the growth of Hep 3B cells in response to AR-A014418 was evaluated. As shown in Fig. 5A, AR-A014418 suppressed the growth of the cells in a time- and dose-related manner. Twenty μM **3y** and 10 μM AR-A014418 separately inhibited the growth of Hep 3B cells to a similar extent from 0 to 72 h. Although AR-A014418 did not induce apoptosis (Fig. 5B), it triggered autophagy in a time- and dose-related manner at higher tested concentrations of 10–40 μM and longer time (72 h, Fig. 5C). **3y** induced autophagy (Fig. 2D) to a greater extent compared with AR-A014418 (Fig. 5C). Western blot analysis of caspase 3 and LC3-II confirmed that AR-A014418 induced autophagy but not apoptosis (Fig. 5D). To determine if **3y** behaved like AR-A014418 (a GSK-3 inhibitor), GSK-3 activity was examined. As shown in Fig. 5E, there was significant

letter differ, $P < 0.05$. (C) AR-A014418 induced autophagy of Hep 3B cells. After treatment, Hep 3B cells were stained with AO before flow cytometry. The percentages in the figure indicate the proportion of cells (upper two quadrants) with AVOs staining. Data are presented as means ± SEMs. Means without a common letter differ, $P < 0.05$. (D) AR-A014418 increased autophagy marker LC3-II expression. (E) **3y** inhibited phosphor-GSK-3β expression. Whole cell lysates were subjected to Western blot analysis. Anti-caspase 3, anti-LC3, anti-phospho-GSK-3, anti-phospho-GSK-3β, and anti-GSK-3β antibodies served as probes. β-actin served as a loading control. The intensity of each protein expression band of at least three independent experiments was quantified by densitometry normalizing to that of β-actin, with control level arbitrarily set to 1. Data are presented as means ± SEMs. Means in each protein without a common letter differ, $P < 0.05$. Results are representative of three independent experiments.

suppression of expression of phospho-GSK-3β. These data suggest that AR-A014418 acts similarly to **3y** to suppress growth of Hep 3B cells by induction of autophagy and that **3y** behaved like AR-A014418 to suppress expression of phospho-GSK-3β. GSK-3 is a serine/threonine protein kinase that not only decreases glycogen synthase activity but also plays an important role in the signaling transduction involved in regulating cell proliferation and apoptosis. GSK-3 has been suggested to be a major factor in cancer survival since GSK-3 increases the activity of NF-κB, which is overexpressed in many cancers, and is also correlated with chemo-resistance in HCC [118,119]. In addition, reduction in phospho-GSK-3β at Ser9 has been reported to decrease mTOR protein expression, leading to autophagy induction [120,121]. The cytotoxicity of 3y on cancer cells (Figs. 2A, 3A and 5A) may be due to the suppression of phospho-GSK-3β at Ser9, but not total GSK-3β (Fig. 5E). The use of a gene expression signature to predict that **3y** acts like a GSK-3 inhibitor by querying C-Map and determining its molecular action (Fig. 5E) revealed the chemotherapeutic potential of **3y** for the treatment of HCC, and further demonstrates the effectiveness of this novel strategy for rapid drug discovery of cancer therapeutics.

Based on the structure of **3y** and AR-A014418, there are some common points. First, the length of **3y** is almost the same as AR-014418. In addition, the sharp of these two molecules are similar. In the medicinal point of view, urea moiety of AR-A014408 can be replaced by triazole component of the **3y**. Moreover, the thiazole of AR-A014408 is similar to oxazinone group of **3y**. The methylene anisole of AR-014418 in response to ethylene dioxolane of **3y** stands for flexity and hydrophobic property (see Scheme 2).

3. Conclusions

In conclusion, we have synthesized biologically and medicinally important 1,4 disubstituted 1,2,3-triazole analogues containing 2*H*-1,4-benzoxazin-3(4*H*)-one and their derivatives (**3a-3ab**) via 1,3-dipolar cycloaddition using catalytic amount of CuI in excellent product yields. Among these novel compounds, **3y** exhibits cytotoxicity on human HCC Hep 3B cells but is relatively safe to human normal HUVEC cells. Compared to the HCC-targeted therapy Sorafenib, **3y** was found to inhibit the growth of and induce apoptosis and autophagy of Hep 3B cells at a lower dosage for a shorter period of time. Furthermore, coadministration of curcumin increased **3y**-induced cytotoxicity by further induction of autophagy. AR-A014418, an inhibitor of GSK-3, was predicted to display a similar biological function of **3y** by using gene expression signatures of **3y** to query C-Map. Further experiments demonstrate that AR-A014418 indeed behaves like **3y** to exhibit a cytotoxic effect by induction of autophagy, and **3y** also behaves like AR-A014418 to suppress expression of phospho-GSK-3β. Our results suggest that **3y** may have potential as a therapeutic agent in the treatment of HCC, and the proposed novel gene screening platform is an ideal alternative methodology to successfully identify novel synthetic compounds for treatments of human cancers.

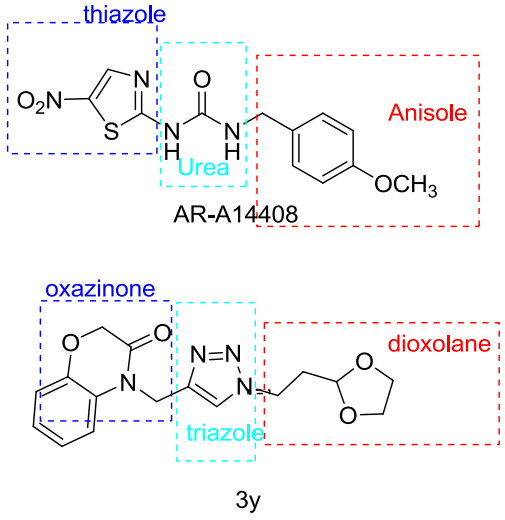

Scheme 2. The structure similarity of **3y** and AR-A014418.

4. Experimental section

4.1. Cell culture and treatment

Human HCC Hep 3B cells and human colorectal cancer HT-29 cells (American Type Culture Collection, Rockville, MD) were maintained in complete Dulbecco's modified Eagle medium (DMEM; GIBCO BRL, Gaithersburg, MD) containing 10% fetal bovine serum (FBS; GIBCO BRL). Human HCC Hep 3B cell line was isolated from a primary tumor obtained from an 8-year-old black male with hepatocellular carcinoma [7]. Human colorectal cancer HT-29 cell line was isolated from a primary tumor from a 44-year-old Caucasian female with colorectal adenocarcinoma in 1964 [122]. HUVEC (a gift from Dr. Ying-Ray Lee, Department of Medical Research, Ditmanson Medical Foundation, Chia-Yi Christian Hospital, Chia-Yi, Taiwan) were cultured with EGM-2 Single Quots (Clonetics, Lonza Walkersville, MD) containing 2% FBS (Clonetics), 0.1% heparin (Clonetics), 0.1% GA-10000 (Clonetics), 0.4% hFGF-B (Clonetics), 0.1% R^3-IGF-1 (Clonetics), 0.1% VEGF (Clonetics), 0.04% hydrocortisone (Clonetics), and 0.1% ascorbic acid (Clonetics). Both cells were maintained in a humidified atmosphere of 5% CO_2 and incubated at 37 °C. Novel synthetic compounds and Sorafenib (Nexavar®) stored at −20 °C were dissolved in 0.1% DMSO (Sigma, St. Louis, MO) before experiment. Control cells were cultured in complete DMEM containing vehicle (0.1% DMSO; this concentration was tested and revealed to be nontoxic to the cells).

4.2. Cell growth assay

The growth of cells was determined using a MTT (Sigma) modified colorimetric assay [107]. After treatment, DMEM containing curcumin, drugs or compounds were removed to avoid color interference in the MTT assay. In the MTT assay, the yellow color was taken up by live cells which then turned purple in color due to the formation of formazan. The absorbance of each well was determined at 590 nm in an ELISA Reader (MRX II, Thermo Fisher Scientific Inc., Waltham, MA). The concentration of each compound was tested in eight replicates. Viability of compound-treated cells was expressed as a percentage of population growth relative to that of untreated control cells. Cell death was calculated as a percentage of inhibition as follows: % inhibition = (1 - mean experimental absorbance/mean control absorbance) × 100. The values of 50% inhibitory concentrations (IC_{50}) were calculated [107].

4.3. Cell cycle determination

Apoptosis was measured by the accumulation of sub-G1 DNA content in the cells since apoptosis-induced fragmented DNA in membrane-bound vesicles increased the hypodiploid (<2N) peak [107]. After treatment, the cells fixed in 70% ethanol (Sigma) were incubated with 40 μg/mL PI (Sigma) and 0.25 μg/mL RNase A (AMRESCO Inc., Solon, OH) for 30 min at room temperature. The PI-stained cells were sorted based on their DNA content in a FACScan flow cytometer (Becton Dickson, Mountain View, CA) [107,123]. Results were analyzed with the Windows Multiple Document

Interface software for Flow Cytometry (WinMDI 2.8, Scripps Research Institute, San Diego, CA).

4.4. Determination of autophagy by formation of acidic vesicular organelles (AVOs)

Autophagy requires formation of autophagosomes, which therefore fuse with endosomes/lysosomes to form mature acidified autolysosomes [124], which can be quantified by staining cells with acridine orange (Sigma) and examining the green and red fluorescence by flow cytometry [125]. After treatment, the cells stained with 1.5 μg/mL AO in the dark for 15 min were detached by trypsinization and sorted by FACScan flow cytometer (Becton Dickson, Mountain View, CA) [126].

4.5. Western blot analysis

Protein contents of whole cell lysates were determined using protein assay kit (Bio-Rad, Hercules, CA). SDS-PAGE was performed using 10–12% polyacrylamide with running buffer (25 mM Tris, 192 mM glycine, and 3.5 mM SDS, pH 8.3). The protein bands on polyacrylamide gels were electrophoretically transferred to polyvinylidene fluoride membranes (Millipore, Bedford, MA). The membranes were then blocked with TBST (20 mM Tris, 137 mM NaCl, and 0.05% Tween-20, pH 7.4) containing 5% skim milk at room temperature for 2 h. The membranes were then probed with a primary antibody and a secondary HRP-conjugate goat anti-rabbit (1:5000) antibody (Millipore Corp., Billerica, MA). The primary antibodies were obtained from the following sources: rabbit anti-LC3B antibody was obtained from Abcam (Cambridge Science Park, UK); Rabbit anti-caspase 3, rabbit anti-phospho-GSK-3α/β (Ser21/9), and rabbit anti-GSK-3β antibodies were obtained from Cell Signaling Technology, Inc. (Danvers, MA). Protein signals were visualized by exposing to X-ray film (Kodak, Rochester, NY) after staining with enhanced chemiluminescence reagents (PerkinElmer, Boston, MA).

4.6. Biological function prediction of **3y** using connectivity map

Connectivity Map is a database hosting gene expression profiles of many FDA-approved drugs and other small molecules [87,88]. The L1000 profiling, a high-throughput gene expression profiling technology [127] allowing effective acquisition of up- or down-regulated genes in cancer cells at one time, was performed by Genometry Inc. (MA, USA). About 1000 “landmark genes” per sample were examined, which closely represents the data obtained using a conventional microarray. As previously described [89], Hep 3B cells were treated with **3y** (0–10 μM) for 6 or 24 h and then subjected to L1000 profiling. The obtained gene expression signature was analyzed by comparing with the Connectivity Map 2.0 (http://www.broadinstitute.org/cmap) to predict functional connections.

4.7. Interaction of two compounds

The effect of the interaction of curcumin with **3y** on cell growth inhibition was calculated using the method described by Jin [128]. Synergism, antagonism, and additivity were defined as $q > 1.15$, $q < 0.85$, and between 0.85 and 1.15, respectively.

4.8. Statistics

The results were expressed as means ± standard errors of the means (SEMs). The data were analyzed by one-way ANOVA. Differences among groups were analyzed by Duncan's multiple range tests (SPSS software, version 14.0). Significant differences were considered to be $P < 0.05$.

Acknowledgments

We are thankful to Professor Chung-Wai Shiau, Institute of Biopharmaceutical Sciences, National Yang-Ming University, Taipei, Taiwan, for editing the manuscript. Financial support for this work from the National Science Council, Taiwan (NSC 98-2313-B-003-002-MY3 and NSC 101-2313-B-003-002-MY3), the Ministry of Science and Technology, Taiwan (MOST 105–3011-B010-001, MOST 104-2627-B-010-001, and MOST 104-2320-B-003-007), and the National Taiwan Normal University (99T3030-2, 99-D, 100-D-06, and 103-07-C) is gratefully acknowledged.

Appendix A. Supplementary data

Supplementary data related to this article can be found at http://dx.doi.org/10.1016/j.ejmech.2017.03.034.

References

[1] M.J. Genin, D.A. Allwine, D.J. Anderson, M.R. Barbachyn, D.E. Emmert, S.A. Garmon, D.R. Graber, K.C. Grega, J.B. Hester, D.K. Hutchinson, J. Morris, R.J. Reischer, C.W. Ford, G.E. Zurenko, J.C. Hamel, R.D. Schaadt, D. Stapert, B.H. Yagi, Substituent effects on the antibacterial activity of nitrogen-carbon-linked (azolylphenyl)oxazolidinones with expanded activity against the fastidious gram-negative organisms *Haemophilus influenzae* and *Moraxella catarrhalis*, J. Med. Chem. 43 (2000) 953–970.
[2] D.R. Buckle, C.J. Rockell, H. Smith, B.A. Spicer, Studies on 1,2,3-triazoles. 13. (Piperazinylalkoxy) [1]benzopyrano[2,3-d]-1,2,3-triazol-9(1H)-ones with combined H1-antihistamine and mast cell stabilizing properties, J. Med. Chem. 29 (1986) 2262–2267.
[3] J.C. Fung-Tomc, E. Huczko, B. Minassian, D.P. Bonner, *In vitro* activity of a new oral triazole, BMS-207147 (ER-30346), Antimicrob. Agents Chemother. 42 (1998) 313–318.
[4] C.B. Vicentini, V. Brandolini, M. Guarneri, P. Giori, Pyrazolo[3,4-d][1,2,3]triazole-1-carboxamides and 5-alkylaminopyrazolo[3,4-d]oxazoles: synthesis and evaluation of the *in vitro* antifungal activity, Farmaco 47 (1992) 1021–1034.
[5] S. Palhagen, R. Canger, O. Henriksen, J.A. van Parys, M.E. Riviere, M.A. Karolchyk, Rufinamide: a double-blind, placebo-controlled proof of principle trial in patients with epilepsy, Epilepsy Res. 43 (2001) 115–124.
[6] R. Alvarez, S. Velazquez, A. San-Felix, S. Aquaro, E. De Clercq, C.F. Perno, A. Karlsson, J. Balzarini, M.J. Camarasa, 1,2,3-Triazole-[2',5'-bis-O-(tert-butyldimethylsilyl)-beta-D- ribofuranosyl]-3'-spiro-5“-(4”-amino-1“,2”-oxathiole 2“,2”-dioxide) (TSAO) analogues: synthesis and anti-HIV-1 activity, J. Med. Chem. 37 (1994) 4185–4194.
[7] N. Gouault, J.F. Cupif, A. Sauleau, M. David, γ-Methyl-substituted-γ-butyrolactones: solid-phase synthesis employing a cyclisation-cleavage strategy, Tetrahedron Lett. 41 (2000) 7293–7297.
[8] S.K. Mamidyala, M.G. Finn, *In situ* click chemistry: probing the binding landscapes of biological molecules, Chem. Soc. Rev. 39 (2010) 1252–1261.
[9] J.C. Jewett, C.R. Bertozzi, Cu-free click cycloaddition reactions in chemical biology, Chem. Soc. Rev. 39 (2010) 1272–1279.
[10] Y. Hua, A.H. Flood, Click chemistry generates privileged CH hydrogen-bonding triazoles: the latest addition to anion supramolecular chemistry, Chem. Soc. Rev. 39 (2010) 1262–1271.
[11] C.O. Kappe, E. Van der Eycken, Click chemistry under non-classical reaction conditions, Chem. Soc. Rev. 39 (2010) 1280–1290.
[12] B.R. Buckley, S.E. Dann, H. Heaney, Experimental evidence for the involvement of dinuclear alkynylcopper(I) complexes in alkyne-azide chemistry, Chemistry 16 (2010) 6278–6284.
[13] C. Spiteri, J.E. Moses, Copper-catalyzed azide-alkyne cycloaddition: regioselective synthesis of 1,4,5-trisubstituted 1,2,3-triazoles, Angew. Chem. Int. Ed. Engl. 49 (2010) 31–33.
[14] C.W. Tornoe, C. Christensen, M. Meldal, Peptidotriazoles on solid phase: [1,2,3]-triazoles by regiospecific copper(i)-catalyzed 1,3-dipolar cycloadditions of terminal alkynes to azides, J. Org. Chem. 67 (2002) 3057–3064.
[15] V.V. Rostovtsev, L.G. Green, V.V. Fokin, K.B. Sharpless, A stepwise huisgen cycloaddition process: copper(I)-catalyzed regioselective “ligation” of azides and terminal alkynes, Angew. Chem. Int. Ed. Engl. 41 (2002) 2596–2599.
[16] M. Meldal, C.W. Tornoe, Cu-catalyzed azide-alkyne cycloaddition, Chem. Rev. 108 (2008) 2952–3015.
[17] R. Li, D.J. Jansen, A. Datta, Intramolecular azide-alkyne [3 + 2] cycloaddition: versatile route to new heterocyclic structural scaffolds, Org. Biomol. Chem. 7 (2009) 1921–1930.
[18] S. Chandrasekhar, M. Seenaiah, A. Kumar, C.R. Reddy, S.K. Mamidyala,

C.G. Kumar, S. Balasubramanian, Intramolecular copper(I)-catalyzed 1,3-dipolar cycloaddition of azido-alkynes:synthesis of triazolo-benzoxazepine derivatives and their biological evaluation, Tetrahedron Lett. 52 (2011) 806–808.
[19] D. Kumar, V.B. Reddy, R.S. Varma, A facile and regioselective synthesis of 1,4-disubstituted 1,2,3-triazoles using click chemistry, Tetrahedron Lett. 50 (2009) 2065–2068.
[20] C. Chowdhury, S. Mukherjee, B. Das, B. Achari, Expedient and rapid synthesis of 1,2,3-triazolo[5,1-c]morpholines through palladium-copper catalysis, J. Org. Chem. 74 (2009) 3612–3615.
[21] C. Chowdhury, A.K. Sasmal, P.K. Dutta, Efficient synthesis of [1,2,3]triazolo [5,1-c][1,4]benzoxazines through palladium–copper catalysis, Tetrahedron Lett. 50 (2009) 2678–2681.
[22] H. Nandivada, X. Jiang, J. Lahann, Click chemistry: versatility and control in the hands of materials scientists, J. Adv. Mater 19 (2007) 2197–2208.
[23] S. Roper, M.H. Franz, R. Wartchow, H.M. Hoffmann, Fused triazoles via tandem reactions of activated Cinchona alkaloids with azide ion. Second Cinchona rearrangement exemplified, Org. Lett. 5 (2003) 2773–2776.
[24] J. Panteleev, K. Geyer, A. Aguilar-Aguilar, L. Wang, M. Lautens, C-H bond functionalization in the synthesis of fused 1,2,3-triazoles, Org. Lett. 12 (2010) 5092–5095.
[25] A.I. Oliva, U. Christmann, D. Font, F. Cuevas, P. Ballester, H. Buschmann, A. Torrens, S. Yenes, M.A. Pericas, Intramolecular azide-alkyne cycloaddition for the fast assembly of structurally diverse, tricyclic 1,2,3-triazoles, Org. Lett. 10 (2008) 1617–1619.
[26] V. Sai Sudhir, N.Y. Phani Kumar, R.B. Nasir Baig, S. Chandrasekaran, Facile entry into triazole fused heterocycles via sulfamidate derived azido-alkynes, J. Org. Chem. 74 (2009) 7588–7591.
[27] R.A. Brawn, M. Welzel, J.T. Lowe, J.S. Panek, Regioselective intramolecular dipolar cycloaddition of azides and unsymmetrical alkynes, Org. Lett. 12 (2010) 336–339.
[28] E. Balducci, L. Bellucci, E. Petricci, M. Taddei, A. Tafi, Microwave-assisted intramolecular Huisgen cycloaddition of azido alkynes derived from alpha-amino acids, J. Org. Chem. 74 (2009) 1314–1321.
[29] Y. Angell, K. Burgess, Ring closure to beta-turn mimics via copper-catalyzed azide/alkyne cycloadditions, J. Org. Chem. 70 (2005) 9595–9598.
[30] A. Kamal, N. Shankaraiah, V. Devaiah, K. Laxma Reddy, A. Juvekar, S. Sen, N. Kurian, S. Zingde, Synthesis of 1,2,3-triazole-linked pyrrolobenzodiazepine conjugates employing 'click' chemistry: DNA-binding affinity and anticancer activity, Bioorg. Med. Chem. Lett. 18 (2008) 1468–1473.
[31] A.K. Feldman, B. Colasson, V.V. Fokin, One-pot synthesis of 1,4-disubstituted 1,2,3-triazoles from in situ generated azides, Org. Lett. 6 (2004) 3897–3899.
[32] S. Velazquez, R. Alvarez, C. Perez, F. Gago, E. De Clercq, J. Balzarini, M.J. Camarasa, Regiospecific synthesis and anti-human immunodeficiency virus activity of novel 5-substituted N-alkylcarbamoyl and N,N-dialkylcarbamoyl 1,2,3-triazole-TSAO analogues, Antivir. Chem. Chemother. 9 (1998) 481–489.
[33] W. Yan, Q. Wang, Y. Chen, J.L. Petersen, X. Shi, Iron-catalyzed C-O bond activation for the synthesis of propargyl-1,2,3-triazoles and 1,1-bis-triazoles, Org. Lett. 12 (2010) 3308–3311.
[34] B. Sreedhar, P.S. Reddy, V.R. Krishna, Regioselective synthesis of 1,4-disubstituted 1,2,3-triazoles via three-component coupling of secondary alcohols, TMSN3 and alkynes, Tetrahedron Lett. 2007 48 (48) (2007) 5831–5834.
[35] F. Shi, J.P. Waldo, Y. Chen, R.C. Larock, Benzyne click chemistry: synthesis of benzotriazoles from benzynes and azides, Org. Lett. 10 (2008) 2409–2412.
[36] H. Juwarker, J.M. Lenhardt, J.C. Castillo, E. Zhao, S. Krishnamurthy, R.M. Jamiolkowski, K.H. Kim, S.L. Craig, Anion binding of short, flexible aryl triazole oligomers, J. Org. Chem. 74 (2009) 8924–8934.
[37] K.D. Bodine, D.Y. Gin, M.S. Gin, Synthesis of readily modifiable cyclodextrin analogues via cyclodimerization of an alkynyl-azido trisaccharide, J. Am. Chem. Soc. 126 (2004) 1638–1639.
[38] A.R. Bogdan, K. James, Efficient access to new chemical space through flow-construction of druglike macrocycles through copper-surface-catalyzed azide-alkyne cycloaddition reactions, Chemistry 16 (2010) 14506–14512.
[39] S. Dorner, B. Westermann, A short route for the synthesis of “sweet” macrocycles via a click-dimerization-ring-closing metathesis approach, Chem. Commun. (2005) 2852–2854.
[40] L.A. Marcaurelle, E. Comer, S. Dandapani, J.R. Duvall, B. Gerard, S. Kesavan, M.D.t. Lee, H. Liu, J.T. Lowe, J.C. Marie, C.A. Mulrooney, B.A. Pandya, A. Rowley, T.D. Ryba, B.C. Suh, J. Wei, D.W. Young, L.B. Akella, N.T. Ross, Y.L. Zhang, D.M. Fass, S.A. Reis, W.N. Zhao, S.J. Haggarty, M. Palmer, M.A. Foley, An aldol-based build/couple/pair strategy for the synthesis of medium- and large-sized rings: discovery of macrocyclic histone deacetylase inhibitors, J. Am. Chem. Soc. 132 (2010) 16962–16976.
[41] J.F. Billing, U.J. Nilsson, C2-symmetric macrocyclic carbohydrate/amino acid hybrids through copper(I)-catalyzed formation of 1,2,3-triazoles, J. Org. Chem. 70 (2005) 4847–4850.
[42] S. Punna, J. Kuzelka, Q. Wang, M.G. Finn, Head-to-tail peptide cyclodimerization by copper-catalyzed azide-alkyne cycloaddition, Angew. Chem. Int. Ed. Engl. 44 (2005) 2215–2220.
[43] J.H. van Maarseveen, W.S. Horne, M.R. Ghadiri, Efficient route to C2 symmetric heterocyclic backbone modified cyclic peptides, Org. Lett. 7 (2005) 4503–4506.
[44] V.D. Bock, R. Perciaccante, T.P. Jansen, H. Hiemstra, J.H. van Maarseveen, Click chemistry as a route to cyclic tetrapeptide analogues: synthesis of cyclo-[Pro-Val-psi(triazole)-Pro-Tyr], Org. Lett. 8 (2006) 919–922.
[45] K. Oh, Z. Guan, A convergent synthesis of new beta-turn mimics by click chemistry, Chem. Commun. (2006) 3069–3071.
[46] P. Schmieder, R. Kuhne, J. Rademann, Metal-free, regioselective triazole ligations that deliver locked cis peptide mimetics, Angew. Chem. Int. Ed. Engl. 48 (2009) 5042–5045.
[47] D. Bonnet, S. Riche, S. Loison, R. Dagher, M.C. Frantz, L. Boudier, R. Rahmeh, B. Mouillac, J. Haiech, M. Hibert, Solid-phase organic tagging resins for labeling biomolecules by 1,3-dipolar cycloaddition: application to the synthesis of a fluorescent non-peptidic vasopressin receptor ligand, Chemistry 14 (2008) 6247–6254.
[48] A. Tam, U. Arnold, M.B. Soellner, R.T. Raines, Protein prosthesis: 1,5-disubstituted[1,2,3]triazoles as cis-peptide bond surrogates, J. Am. Chem. Soc. 129 (2007) 12670–12671.
[49] D.J. Guerin, S.J. Miller, Asymmetric azidation-cycloaddition with open-chain peptide-based catalysts. A sequential enantioselective route to triazoles, J. Am. Chem. Soc. 124 (2002) 2134–2136.
[50] M. Whiting, J. Muldoon, Y.C. Lin, S.M. Silverman, W. Lindstrom, A.J. Olson, H.C. Kolb, M.G. Finn, K.B. Sharpless, J.H. Elder, V.V. Fokin, Inhibitors of HIV-1 protease by using in situ click chemistry, Angew. Chem. Int. Ed. Engl. 45 (2006) 1435–1439.
[51] N.A. Al-Masoudi, Y.A. Al-Soud, Synthesis of 1'–d-glucopyranosyl-1,2,3-triazole-4,5-dimethanol-4,5-bis(isopropylcarbam ate) as potential antineoplastic agent, Tetrahedron Lett. 2002 43 (43) (2002) 4021–4022.
[52] S. Chandrasekhar, C.L. Rao, C. Nagesh, C.R. Reddy, B. Sridhar, Inter and intramolecular copper(I)-catalyzed 1,3-dipolar cycloaddition of azido-alkynes: synthesis of furanotriazole macrocycles, Tetrahedron Lett. 48 (2007) 5869–5872.
[53] B.H. Kuijpers, S. Groothuys, A.B. Keereweer, P.J. Quaedflieg, R.H. Blaauw, F.L. van Delft, F.P. Rutjes, Expedient synthesis of triazole-linked glycosyl amino acids and peptides, Org. Lett. 6 (2004) 3123–3126.
[54] A. Dondoni, P.P. Giovannini, A. Massi, Assembling heterocycle-tethered C-glycosyl and alpha-amino acid residues via 1,3-dipolar cycloaddition reactions, Org. Lett. 6 (2004) 2929–2932.
[55] S. Chittaboina, F. Xie, Q. Wang, One-pot synthesis of triazole-linked glycoconjugates, Tetrahedron Lett. 46 (2005) 2331–2336.
[56] J.M. Aizpurua, I. Azcune, R.M. Fratila, E. Balentova, M. Sagartzazu-Aizpurua, J.I. Miranda, “Click” synthesis of nonsymmetrical bis(1,2,3-triazoles), Org. Lett. 12 (2010) 1584–1587.
[57] S. Hotha, R.I. Anegundi, A.A. Natu, Expedient synthesis of 1,2,3-triazole-fused tetracyclic compounds by intramolecular Huisgen (‘click’) reactions on carbohydrate-derived azido-alkynes, Tetrahedron Lett. 46 (2005) 4585–4588.
[58] S. Cecioni, S. Faure, U. Darbost, I. Bonnamour, H. Parrot-Lopez, O. Roy, C. Taillefumier, M. Wimmerova, J.P. Praly, A. Imberty, S. Vidal, Selectivity among two lectins: probing the effect of topology, multivalency and flexibility of “clicked” multivalent glycoclusters, Chemistry 17 (2011) 2146–2159.
[59] S. Hotha, S. Kashyap, “Click chemistry” inspired synthesis of pseudo-oligosaccharides and amino acid glycoconjugates, J. Org. Chem. 71 (2006) 364–367.
[60] A. Macchiarulo, G. Costantino, D. Fringuelli, A. Vecchiarelli, F. Schiaffella, R. Fringuelli, 1,4-Benzothiazine and 1,4-benzoxazine imidazole derivatives with antifungal activity: a docking study, Bioorg. Med. Chem. 10 (2002) 3415–3423.
[61] P. Smid, H.K. Coolen, H.G. Keizer, R. van Hes, J.P. de Moes, A.P. den Hartog, B. Stork, R.H. Plekkenpol, L.C. Niemann, C.N. Stroomer, M.T. Tulp, H.H. van Stuivenberg, A.C. McCreary, M.B. Hesselink, A.H. Herremans, C.G. Kruse, Synthesis, structure-activity relationships, and biological properties of 1-heteroaryl-4-[omega-(1H-indol-3-yl)alkyl]piperazines, novel potential antipsychotics combining potent dopamine D2 receptor antagonism with potent serotonin reuptake inhibition, J. Med. Chem. 48 (2005) 6855–6869.
[62] T.B. Lanni Jr., K.L. Greene, C.N. Kolz, K.S. Para, M. Visnick, J.L. Mobley, D.T. Dudley, T.J. Baginski, M.B. Liimatta, Design and synthesis of phenethyl benzo[1,4]oxazine-3-ones as potent inhibitors of PI3Kinasegamma, Bioorg. Med. Chem. Lett. 17 (2007) 756–760.
[63] R. Fringuelli, D. Pietrella, F. Schiaffella, A. Guarraci, S. Perito, F. Bistoni, A. Vecchiarelli, Anti-Candida albicans properties of novel benzoxazine analogues, Bioorg. Med. Chem. 10 (2002) 1681–1686.
[64] M. Anderluh, J. Cesar, P. Stefanic, D. Kikelj, D. Janes, J. Murn, K. Nadrah, M. Tominc, E. Addicks, A. Giannis, M. Stegnar, M.S. Dolenc, Design and synthesis of novel platelet fibrinogen receptor antagonists with 2H-1,4-benzoxazine-3(4H)-one scaffold. A systematic study, Eur. J. Med. Chem. 40 (2005) 25–49.
[65] M. Scheunemann, D. Sorger, E. Kouznetsova, O. Sabri, R. Schliebs, B. Wenzel, J. Steinbach, Sequential ring-opening of trans-1,4-cyclohexadiene dioxide for an expedient modular approach to 6,7-disubstituted (±)-hexahydro-benzo [1,4]oxazin-3-ones, Tetrahedron Lett. 48 (2007) 5497–5501.
[66] H.M. Niemeyer, Hydroxamic acids (4-hydroxy-1,4-benzoxazin-3-ones), defence chemicals in the gramineae, Phytochem. 1988 27 (27) (1988) 3349–3358.
[67] H.B. Borate, S.R. Maujan, S.P. Sawargave, M.A. Chandavarkar, S.R. Vaiude, V.A. Joshi, R.D. Wakharkar, R. Iyer, R.G. Kelkar, S.P. Chavan, S.S. Kunte, Fluconazole analogues containing 2H-1,4-benzothiazin-3(4H)-one or 2H-1,4-

benzoxazin-3(4H)-one moieties, a novel class of anti-Candida agents, Bioorg. Med. Chem. Lett. 20 (2010) 722–725.
[68] A.R. Li, J. Zhang, J. Greenberg, T. Lee, J. Liu, Discovery of non-glucoside SGLT2 inhibitors, Bioorg. Med. Chem. Lett. 21 (2011) 2472–2475.
[69] F. Schiaffella, A. Macchiarulo, L. Milanese, A. Vecchiarelli, G. Costantino, D. Pietrella, R. Fringuelli, Design, synthesis, and microbiological evaluation of new Candida albicans CYP51 inhibitors, J. Med. Chem. 48 (2005) 7658–7666.
[70] R. Fringuelli, N. Giacche, L. Milanese, E. Cenci, A. Macchiarulo, A. Vecchiarelli, G. Costantino, F. Schiaffella, Bulky 1,4-benzoxazine derivatives with antifungal activity, Bioorg. Med. Chem. 17 (2009) 3838–3846.
[71] J.S. Lee, I.S. Chu, J. Heo, D.F. Calvisi, Z. Sun, T. Roskams, A. Durnez, A.J. Demetris, S.S. Thorgeirsson, Classification and prediction of survival in hepatocellular carcinoma by gene expression profiling, Hepatology 40 (2004) 667–676.
[72] A.X. Zhu, Hepatocellular carcinoma: are we making progress? Cancer Invest. 21 (2003) 418–428.
[73] A.X. Zhu, Systemic therapy of advanced hepatocellular carcinoma: how hopeful should we be? Oncologist 11 (2006) 790–800.
[74] A.L. Cheng, Y.K. Kang, Z. Chen, C.J. Tsao, S. Qin, J.S. Kim, R. Luo, J. Feng, S. Ye, T.S. Yang, J. Xu, Y. Sun, H. Liang, J. Liu, J. Wang, W.Y. Tak, H. Pan, K. Burock, J. Zou, D. Voliotis, Z. Guan, Efficacy and safety of sorafenib in patients in the Asia-Pacific region with advanced hepatocellular carcinoma: a phase III randomised, double-blind, placebo-controlled trial, Lancet Oncol. 10 (2009) 25–34.
[75] L. Lang, FDA approves sorafenib for patients with inoperable liver cancer, Gastroenterology 134 (2008) 379.
[76] C. Gridelli, P. Maione, F. Del Gaizo, G. Colantuoni, C. Guerriero, C. Ferrara, D. Nicolella, D. Comunale, A. De Vita, A. Rossi, Sorafenib and sunitinib in the treatment of advanced non-small cell lung cancer, Oncologist 12 (2007) 191–200.
[77] M. Beeram, A. Patnaik, E.K. Rowinsky, Raf: a strategic target for therapeutic development against cancer, J. Clin. Oncol. 23 (2005) 6771–6790.
[78] S.M. Wilhelm, C. Carter, L. Tang, D. Wilkie, A. McNabola, H. Rong, C. Chen, X. Zhang, P. Vincent, M. McHugh, Y. Cao, J. Shujath, S. Gawlak, D. Eveleigh, B. Rowley, L. Liu, L. Adnane, M. Lynch, D. Auclair, I. Taylor, R. Gedrich, A. Voznesensky, B. Riedl, L.E. Post, G. Bollag, P.A. Trail, BAY 43-9006 exhibits broad spectrum oral antitumor activity and targets the RAF/MEK/ERK pathway and receptor tyrosine kinases involved in tumor progression and angiogenesis, Cancer Res. 64 (2004) 7099–7109.
[79] Y.H. Hwang, J.Y. Choi, S. Kim, E.S. Chung, T. Kim, S.S. Koh, B. Lee, S.H. Bae, J. Kim, Y.M. Park, Over-expression of c-raf-1 proto-oncogene in liver cirrhosis and hepatocellular carcinoma, Hepatol. Res. 29 (2004) 113–121.
[80] M.A. Avila, C. Berasain, B. Sangro, J. Prieto, New therapies for hepatocellular carcinoma, Oncogene 25 (2006) 3866–3884.
[81] J.M. Llovet, S. Ricci, V. Mazzaferro, P. Hilgard, E. Gane, J.F. Blanc, A.C. de Oliveira, A. Santoro, J.L. Raoul, A. Forner, M. Schwartz, C. Porta, S. Zeuzem, L. Bolondi, T.F. Greten, P.R. Galle, J.F. Seitz, I. Borbath, D. Haussinger, T. Giannaris, M. Shan, M. Moscovici, D. Voliotis, J. Bruix, Sorafenib in advanced hepatocellular carcinoma, N. Engl. J. Med. 359 (2008) 378–390.
[82] B. Xie, D.H. Wang, S.J. Spechler, Sorafenib for treatment of hepatocellular carcinoma: a systematic review, Dig. Dis. Sci. 57 (2012) 1122–1129.
[83] C. Widakowich, G. de Castro Jr., E. de Azambuja, P. Dinh, A. Awada, Review: side effects of approved molecular targeted therapies in solid cancers, Oncologist 12 (2007) 1443–1455.
[84] Y. Je, F.A. Schutz, T.K. Choueiri, Risk of bleeding with vascular endothelial growth factor receptor tyrosine-kinase inhibitors sunitinib and sorafenib: a systematic review and meta-analysis of clinical trials, Lancet Oncol. 10 (2009) 967–974.
[85] T.K. Choueiri, F.A. Schutz, Y. Je, J.E. Rosenberg, J. Bellmunt, Risk of arterial thromboembolic events with sunitinib and sorafenib: a systematic review and meta-analysis of clinical trials, J. Clin. Oncol. 28 (2010) 2280–2285.
[86] S. Wu, J.J. Chen, A. Kudelka, J. Lu, X. Zhu, Incidence and risk of hypertension with sorafenib in patients with cancer: a systematic review and meta-analysis, Lancet Oncol. 9 (2008) 117–123.
[87] J. Lamb, E.D. Crawford, D. Peck, J.W. Modell, I.C. Blat, M.J. Wrobel, J. Lerner, J.P. Brunet, A. Subramanian, K.N. Ross, M. Reich, H. Hieronymus, G. Wei, S.A. Armstrong, S.J. Haggarty, P.A. Clemons, R. Wei, S.A. Carr, E.S. Lander, T.R. Golub, The connectivity map: using gene-expression signatures to connect small molecules, genes, and disease, Science 313 (2006) 1929–1935.
[88] J. Lamb, The connectivity map: a new tool for biomedical research, Nat. Rev. Cancer 7 (2007) 54–60.
[89] C.T. Yeh, A.T. Wu, P.M. Chang, K.Y. Chen, C.N. Yang, S.C. Yang, C.C. Ho, C.C. Chen, Y.L. Kuo, P.Y. Lee, Y.W. Liu, C.C. Yen, M. Hsiao, P.J. Lu, J.M. Lai, L.S. Wang, C.H. Wu, J.F. Chiou, P.C. Yang, C.Y. Huang, Trifluoperazine, an antipsychotic agent, inhibits cancer stem cell growth and overcomes drug resistance of lung cancer, Am. J. Respir. Crit. Care Med. 186 (2012) 1180–1188.
[90] C.T. Yeh, C.L. Su, C.Y. Huang, J.K. Lin, W.H. Lee, P.M. Chang, Y.L. Kuo, Y.W. Liu, L.S. Wang, C.H. Wu, Y.S. Shieh, Y.H. Jan, Y.J. Chuang, M. Hsiao, A.T. Wu, A preclinical evaluation of antimycin a as a potential antilung cancer stem cell agent, Evid. Based Complement. Altern. Med. 2013 (2013) 910451.
[91] D. Hanahan, R.A. Weinberg, Hallmarks of cancer: the next generation, Cell 144 (2011) 646–674.
[92] J.J. Liu, M. Lin, J.Y. Yu, B. Liu, J.K. Bao, Targeting apoptotic and autophagic pathways for cancer therapeutics, Cancer Lett. 300 (2011) 105–114.
[93] Y. Kondo, S. Kondo, Autophagy and cancer therapy, Autophagy 2 (2006) 85–90.
[94] Y. Kondo, T. Kanzawa, R. Sawaya, S. Kondo, The role of autophagy in cancer development and response to therapy, Nat. Rev. Cancer 5 (2005) 726–734.
[95] Z.J. Yang, C.E. Chee, S. Huang, F.A. Sinicrope, The role of autophagy in cancer: therapeutic implications, Mol. Cancer Ther. 10 (2011) 1533–1541.
[96] R.A. Sharma, A.J. Gescher, W.P. Steward, Curcumin: the story so far, Eur. J. Cancer 41 (2005) 1955–1968.
[97] B.B. Aggarwal, S. Shishodia, Molecular targets of dietary agents for prevention and therapy of cancer, Biochem. Pharmacol. 71 (2006) 1397–1421.
[98] R. Bhat, Y. Xue, S. Berg, S. Hellberg, M. Ormo, Y. Nilsson, A.C. Radesater, E. Jerning, P.O. Markgren, T. Borgegard, M. Nylof, A. Gimenez-Cassina, F. Hernandez, J.J. Lucas, J. Diaz-Nido, J. Avila, Structural insights and biological effects of glycogen synthase kinase 3-specific inhibitor AR-A014418, J. Biol. Chem. 278 (2003) 45937–45945.
[99] C. Ramesh, B.R. Raju, V. Kavala, C.-W. Kuo, C.-F. Yao, A simple and facile route for the synthesis of 2H-1,4-benzoxazin-3-(4H)-ones via reductive cyclization of 2-(2-nitrophenoxy)acetonitrile adducts in the presence of Fe/acetic acid, Tetrahedron 2011 67 (67) (2011) 1187–1192.
[100] L.S. Campbell-Verduyn, L. Mirfeizi, R.A. Dierckx, P.H. Elsinga, B.L. Feringa, Phosphoramidite accelerated copper(i)-catalyzed [3 + 2] cycloadditions of azides and alkynes, Chem. Commun. (2009) 2139–2141.
[101] S.G. Alvarez, M.T. Alvarez, A practical procedure for the synthesis of alkyl azides at ambient temperature in dimethyl sulfoxide in high purity and yield, Synthesis 4 (1997) 413–414.
[102] P. Ramirez-Lopez, M.C. de la Torre, H.E. Montenegro, M. Asenjo, M.A. Sierra, A straightforward synthesis of tetrameric estrone-based macrocycles, Org. Lett. 10 (2008) 3555–3558.
[103] CCDC numbers of 3a is 871251, The Data Can Be Obtained Free of Charge from Cambridge Crystallographic Data Center via. www.ccdc.cam.ac.uk/datarequest/cif.
[104] G.K. Abou-Alfa, L. Schwartz, S. Ricci, D. Amadori, A. Santoro, A. Figer, J. De Greve, J.Y. Douillard, C. Lathia, B. Schwartz, I. Taylor, M. Moscovici, L.B. Saltz, Phase II study of sorafenib in patients with advanced hepatocellular carcinoma, J. Clin. Oncol. 24 (2006) 4293–4300.
[105] F.H. Igney, P.H. Krammer, Death and anti-death: tumour resistance to apoptosis, Nat. Rev. Cancer 2 (2002) 277–288.
[106] G. Wickman, L. Julian, M.F. Olson, How apoptotic cells aid in the removal of their own cold dead bodies, Cell Death Differ. 19 (2012) 735–742.
[107] J.C. Lee, C.H. Lee, C.L. Su, C.W. Huang, H.S. Liu, C.N. Lin, S.J. Won, Justicidin A decreases the level of cytosolic Ku70 leading to apoptosis in human colorectal cancer cells, Carcinogenesis 26 (2005) 1716–1730.
[108] A. Shehzad, F. Wahid, Y.S. Lee, Curcumin in cancer chemoprevention: molecular targets, pharmacokinetics, bioavailability, and clinical trials, Arch. Pharm. 343 (2010) 489–499.
[109] Y. Sadzuka, M. Nagamine, T. Toyooka, Y. Ibuki, T. Sonobe, Beneficial effects of curcumin on antitumor activity and adverse reactions of doxorubicin, Int. J. Pharm. 432 (2012) 42–49.
[110] W. Roth, J.C. Reed, Apoptosis and cancer: when BAX is TRAILing away, Nat. Med. 8 (2002) 216–218.
[111] S.H. Lan, S.Y. Wu, R. Zuchini, X.Z. Lin, I.J. Su, T.F. Tsai, Y.J. Lin, C.T. Wu, H.S. Liu, Autophagy suppresses tumorigenesis of hepatitis B Virus-associated hepatocellular carcinoma through degradation of microRNA-224, Hepatology 59 (2014) 505–517.
[112] H. Qian, Y. Yang, X. Wang, Curcumin enhanced adriamycin-induced human liver-derived hepatoma G2 cell death through activation of mitochondria-mediated apoptosis and autophagy, Eur. J. Pharm. Sci. 43 (2011) 125–131.
[113] K. Xiao, J. Jiang, C. Guan, C. Dong, G. Wang, L. Bai, J. Sun, C. Hu, C. Bai, Curcumin induces autophagy via activating the AMPK signaling pathway in lung adenocarcinoma cells, J. Pharmacol. Sci. 123 (2013) 102–109.
[114] A. Goel, A.B. Kunnumakkara, B.B. Aggarwal, Curcumin as “curecumin”: from kitchen to clinic, Biochem. Pharmacol. 75 (2008) 787–809.
[115] A.B. Kunnumakkara, P. Anand, B.B. Aggarwal, Curcumin inhibits proliferation, invasion, angiogenesis and metastasis of different cancers through interaction with multiple cell signaling proteins, Cancer Lett. 269 (2008) 199–225.
[116] H. Hatcher, R. Planalp, J. Cho, F.M. Torti, S.V. Torti, Curcumin: from ancient medicine to current clinical trials, Cell. Mol. Life Sci. 65 (2008) 1631–1652.
[117] S.C. Gupta, G. Kismali, B.B. Aggarwal, Curcumin, a component of turmeric: from farm to pharmacy, Biofactors 39 (2013) 2–13.
[118] J.O. Ban, D.H. Kwak, J.H. Oh, E.J. Park, M.C. Cho, H.S. Song, M.J. Song, S.B. Han, D.C. Moon, K.W. Kang, J.T. Hong, Suppression of NF-kappaB and GSK-3beta is involved in colon cancer cell growth inhibition by the PPAR agonist troglitazone, Chem. Biol. Interact. 188 (2010) 75–85.
[119] M. Frau, F. Biasi, F. Feo, R.M. Pascale, Prognostic markers and putative therapeutic targets for hepatocellular carcinoma, Mol. Asp. Med. 31 (2010) 179–193.
[120] C. Zhang, B. Hou, S. Yu, Q. Chen, N. Zhang, H. Li, HGF alleviates high glucose-induced injury in podocytes by GSK3beta inhibition and autophagy restoration, Biochim. Biophys. Acta 1863 (2016) 2690–2699.
[121] X. Zhang, G.M. Howell, L. Guo, R.D. Collage, P.A. Loughran, B.S. Zuckerbraun, M.R. Rosengart, CaMKIV-dependent preservation of mTOR expression is required for autophagy during lipopolysaccharide-induced inflammation and acute kidney injury, J. Immunol. 193 (2014) 2405–2415.
[122] T.R. Chen, D. Drabkowski, R.J. Hay, M. Macy, W. Peterson Jr., WiDr is a

derivative of another colon adenocarcinoma cell line, HT-29, Cancer Genet. Cytogenet 27 (1987) 125–134.
[123] C.L. Perkins, G. Fang, C.N. Kim, K.N. Bhalla, The role of Apaf-1, caspase-9, and bid proteins in etoposide- or paclitaxel-induced mitochondrial events during apoptosis, Cancer Res. 60 (2000) 1645–1653.
[124] D.J. Klionsky, A.M. Cuervo, P.O. Seglen, Methods for monitoring autophagy from yeast to human, Autophagy 3 (2007) 181–206.
[125] H. Aoki, Y. Takada, S. Kondo, R. Sawaya, B.B. Aggarwal, Y. Kondo, Evidence that curcumin suppresses the growth of malignant gliomas *in vitro* and *in vivo* through induction of autophagy: role of Akt and extracellular signal-regulated kinase signaling pathways, Mol. Pharmacol. 72 (2007) 29–39.
[126] S. Daido, T. Kanzawa, A. Yamamoto, H. Takeuchi, Y. Kondo, S. Kondo, Pivotal role of the cell death factor BNIP3 in ceramide-induced autophagic cell death in malignant glioma cells, Cancer Res. 64 (2004) 4286–4293.
[127] D. Peck, E.D. Crawford, K.N. Ross, K. Stegmaier, T.R. Golub, J. Lamb, A method for high-throughput gene expression signature analysis, Genome Biol. 7 (2006) R61.
[128] X.F. Huang, S.K. Luo, J. Xu, J. Li, D.R. Xu, L.H. Wang, M. Yan, X.R. Wang, X.B. Wan, F.M. Zheng, Y.X. Zeng, Q. Liu, Aurora kinase inhibitory VX-680 increases Bax/Bcl-2 ratio and induces apoptosis in Aurora-A-high acute myeloid leukemia, Blood 111 (2008) 2854–2865.